Accepted Manuscript

Vascular Endothelial Growth Factor C Disrupts the Endothelial Lymphatic Barrier to Promote Colorectal Cancer Invasion

Carlotta Tacconi, Carmen Correale, Alessandro Gandelli, Antonino Spinelli, Elisabetta Dejana, Silvia D'Alessio, Silvio Danese

PII: S0016-5085(15)00310-8
DOI: 10.1053/j.gastro.2015.03.005
Reference: YGAST 59664

To appear in: *Gastroenterology*
Accepted Date: 2 March 2015

Please cite this article as: Tacconi C, Correale C, Gandelli A, Spinelli A, Dejana E, D'Alessio S, Danese S, Vascular Endothelial Growth Factor C Disrupts the Endothelial Lymphatic Barrier to Promote Colorectal Cancer Invasion, *Gastroenterology* (2015), doi: 10.1053/j.gastro.2015.03.005.

Vascular Endothelial Growth Factor C Disrupts the Endothelial Lymphatic Barrier to Promote Colorectal Cancer Invasion

Carlotta Tacconi[1], Carmen Correale[1], Alessandro Gandelli[1], Antonino Spinelli[1], Elisabetta Dejana[2,3] , Silvia D'Alessio[1*] & Silvio Danese[1*]

[1]Humanitas Clinical and Research Center, IBD Center, Rozzano, Italy

[2]FIRC Institute of Molecular Oncology Foundation (IFOM), Milan, Italy

[3]Department of Biosciences, School of Sciences, University of Milan, Milan, Italy

***Corresponding author**: Dr. Silvia D'Alessio, Humanitas Clinical and Research Center, Division of Gastroenterology, Via Manzoni 113, 20089 Rozzano (MI), Italy; TEL.:+39 02 82245146, FAX: +39 02 82245101. Email: silvia.dalessio@humanitasresearch.it

***Corresponding author**: Dr. Silvio Danese, Humanitas Clinical and Research Center, Division of Gastroenterology, Via Manzoni 56, 20089 Rozzano (MI), Italy; TEL. +39 02 82244771; FAX: +39 02 82245101. Email: silvio.danese@humanitas.it

Condensed title: Lymphangiogenesis hastens CRC-metastases

Funding sources and acknowledgements: This study was supported by grants from the Broad Medical Research Program to S.D.; the Italian Ministry of Health to S.D.; the Cariplo foundation to S.D. and E.D.; the Italian Association for Cancer Research (AIRC) to S.D. and E.D., and the European Community (ITN VESSEL 317250) to E.D.; the Innovative Medicines Initiative (IMI) Joint Undertaking BTCure (115142) to S.D.; the Fondazione Italiana per la Ricerca Sulle Malattie Apparato Digerente (FIRMAD) to S.D.; the European Crohn's and Colitis Organisation (ECCO) to S.DA. The work was conducted in the context, and with the support, of the Fondazione Humanitas per la Ricerca (Rozzano, Italy). We thank Ron Haskell (Viraquest) for his expert technical assistance with adenovirus preparation and Paolo Somma (Humanitas Clinical and Research Center) for helping with the sorting of HILECs. Bronislaw Pytowski (ImClone Systems Inc., New York, New York, USA) kindly provided the VEGFR3 blocking antibody mF431C1.

Author contributions: C.T. designed and performed the research, analyzed the data and wrote the manuscript. C.C. helped with the in vivo experiments. A.G. performed the immunohistochemical staining on human samples. A.S. provided human samples. E.D. provided critical comments to the

manuscript. S.DA. designed and performed the research and reviewed the manuscript. S.D. designed the research and provided critical comments to the manuscript.

Disclosure statement

The authors declare no competing, financial, or personal conflicts of interest.

Abbreviations:

CRC: colorectal cancer

HILEC: human intestinal lymphatic endothelial cell

HIBEC: human intestinal blood endothelial cell

LN: lymphnode

LV: lymphatic vessel

MFI: mean fluorescence intensity

PKI: protein kinase inhibitors

SAR131675: SAR

TEER: transendothelial electrical resistance

VE-Cad: vascular endothelial cadherin

VEGFA: vascular endothelial growth factor A

VEGFC: vascular endothelial growth factor C

VEGFD: vascular endothelial growth factor D

VEGFR2: vascular endothelial growth factor receptor 2

VEGFR3: vascular endothelial growth factor receptor 3

Abstract

Background & Aims: Colorectal cancer (CRC) is highly metastatic. Metastases spread directly into local tissue or invade distant organs via blood and lymphatic vessels, but the role of lymphangiogenesis in CRC progression has not been determined. Lymphangiogenesis is induced via vascular endothelial growth factor C (VEGFC) activation of its receptor, VEGFR3; high levels of VEGFC have been measured in colorectal tumors undergoing lymphangiogenesis, and correlated with metastasis. We investigated VEGFC signaling and lymphatic barriers in human tumor tissues and mice with orthotopic colorectal tumors.

Methods: We performed immunohistochemical, immunoblot, and real-time PCR analyses of colorectal tumor specimens collected from patients; healthy intestinal tissues collected during surgeries of patients without CRC were used as controls. CT26 CRC cells were injected into the distal posterior rectum of BALB/c-nude mice. Mice were given injections of an antibody against VEGFR3 or an adenovirus encoding human VEGFC before orthotopic tumors and metastases formed. Lymph node, lung, and liver tissues were collected and evaluated by flow cytometry. We measured expression of vascular endothelial cadherin (CDH5) on lymphatic vessels in mice and in human intestinal lymphatic endothelial cells.

Results: Levels of podoplanin (a marker of lymphatic vessels), VEGFC, and VEGFR3 were increased in colorectal tumor tissues, compared with controls. Mice that expressed VEGFC from the adenoviral vector had increased lymphatic vessel density and more metastases in lymph nodes, lungs, and livers, compared with control mice. Anti-VEGR3 antibody reduced numbers of lymphatic vessels in colons and prevented metastasis. Expression of VEGFC compromised the lymphatic endothelial barrier in mice and endothelial cells, reducing expression of CDH5, increasing permeability, and increasing trans-endothelial migration by CRC cells. Opposite effects were observed in mice and cells when VEGFR3 was blocked.

Conclusions: VEGFC signaling via VEGFR3 promotes lymphangiogenesis and metastasis by orthotopic colorectal tumors in mice and reduces lymphatic endothelial barrier integrity. Levels of VEGFC and markers of lymphatic vessels are increased in CRC tissues from patients, compared with healthy intestine. Strategies to block VEGFR3 might be developed to prevent CRC metastasis in patients.

KEYWORDS: colon cancer, mouse model, tumor progression, VEGFC

Introduction

Colorectal cancer (CRC) is the second most common cause of cancer-related mortality in the Western world[1]. Although it can spread in a variety of ways, lymphatic vessel (LV) invasion and metastasis are common in CRC early stages[2]. Previous studies have shown that vascular endothelial growth factor (VEGF) family members and their receptors (VEGFR) contribute to lymphangiogenesis and the metastatic process in CRC[2]. In fact, high levels of VEGFC and its receptor have been described to promote tumor-associated LV expansion, thus becoming one of the most efficient pathways in regulating lymphangiogenesis, during CRC dissemination[3-5]. However, functional studies regarding lymphangiogenesis and lymphatic metastasis are still lacking in CRC. The lymphatic system plays critical roles in the maintenance of fluid homeostasis, immune response, and cancer progression[6], and to exert its biological functions it undergoes lymphangiogenesis, a process of growth and expansion of the lymphatic vessels. Lymphangiogenesis is activated by the binding of VEGFC and VEGFD to their receptor VEGFR3[7], even if no association of VEGFD expression has been found with CRC lymphatic spread[8]. Even though VEGFC interacts with VEGFR2, which is primarily involved in the induction of angiogenesis[9], one of the major physiological functions of this growth factor is generally accepted to be the inducer of LV growth[10].

Tumor metastasis is responsible for most cancer related deaths. The metastatic process can be described in several steps which involve the transmigration of cancer cells from the primary tumor into the microvascular or the lymphatic endothelium (intravasation and/or extravasation), and subsequently, the formation of a secondary tumor at a distant targeted organ[11]. The experimental manipulation of VEGFC together with the blocking of VEGFR3 activation has been studied in several cancer animal models, providing functional evidences that VEGFC is able to induce tumor lymphangiogenesis, and concomitantly promote metastasis formation in various distant organs[12-14]. One of the main restrictions of tumor cell intravasation through the lymphatic system is LV integrity[15], which is strictly related to the organization of interendothelial adherens junction proteins. These junctions are formed by the homotypic interaction of vascular endothelial cadherin (VE-Cad)[16]. Upon cell-cell adhesion, cadherin units form a core adhesion complex on adjacent cells via their extracellular domains[16]. In greater detail, the VE-Cad intracellular region forms a complex with an intracellular protein network, including α-, β- and γ-catenin and p120[17], thus contributing to the strength of intracellular adhesion[18]. Phosphorylation of VE-Cad on Tyr residues disrupts endothelial cell adherens junctions by causing the dissociation of catenins from VE-Cad, facilitating the diapedesis of leukocytes and metastatic cancer cells[19]. It has been reported that an aberrant localization of VE-Cad on blood vessels is responsible for cancer cell

intravasation and extravasation, thus increasing the metastatic spread of several tumors, including CRC[19]. VE-Cad expression on the microvascular endothelial cell membrane depends on its internalization and degradation, and one of the mechanisms mediating these two events is the activation of VEGFR2 by its ligand VEGFA[12]. No mechanistic data is however available regarding the role of VEGFR3 signaling on lymphatic endothelial cell adherens junctions during CRC spreading. In the present study, with the use of an orthotopic xenotransplantation mouse model of CRC, we demonstrate that VEGFC binding to VEGFR3 controls the metastatic spread through the maintenance of lymphatic endothelial barrier integrity.

Material and Methods (See also Supplemental Material and Methods)

Patients

Tumoral colon tissues were obtained from surgical specimens of CRC patients at different TNM stages, ranging from pT1N0 to pT4N2bM1b. Healthy tissues from the intestine of patients admitted for bowel resection due to diverticulosis or polyps were used as controls. Specimens were formalin-fixed and paraffin-embedded or frozen in Cryoblock Compound (DiaPath) or frozen on dry ice and stored at −80°C. Human studies were approved by the ethics committee of the Istituto Clinico Humanitas.

Animals and animal handling

Mice used in this study were male BALB/c-Nude (CAnN.Cg-Foxn1nu/Crl) (Charles River Laboratories Italia, Lecco, Italy) 7-11 weeks old. All animals were maintained under pathogen-free conditions. Housing was temperature controlled, with a 12 light/12 dark hour cycle. Procedures involving mice conformed to institutional guidelines in agreement with national and international law and were approved by the ethics committee of the Humanitas Research Hospital.

Preparation of cell suspensions and transanal mucosal injection

CT26 mCherry positive cells were harvested from near-confluent cultures by a brief exposure to 0,5% trypsin and 0,02% EDTA (Lonza). Cells were washed with PBS 1X-/- and analyzed by FACS for mCherry positivity prior to injection. Mice were anesthetized with 100mg/kg ketamine and 50mg/kg xylazine. With the use of a 29-gauge syringe, 15000 CT26 mCherry-positive cells were injected submucosally into the distal posterior rectum in a final volume of 50µl, as previously described[20]. Tumor growth was visually monitored daily. Mice were sacrificed on post-injection day 19.

Statistical analyses

Statistical analyses were performed using GraphPad Prism 4 (GraphPad Software), with a 2-tailed, unpaired Student *t* test or with the ANOVA test with Bonferroni's or Dunnet's Multiple Comparison Test, as appropriate. Data were presented as means ±SD and differences were considered statistically significant when $P \leq 0,05$.

Results

Lymphatic vessel density and the VEGFC/VEGFR3 pathway are altered in human metastatic CRC

Increased lymphatic vessel density in CRC is a key step for metastatic progression[5, 21]. For this reason we first evaluated lymphangiogenesis in colon tissues derived from CRC patients with negative (n=13) or positive (n=13) NM stage, and compared them to healthy controls (n=15). We performed an immunohistochemical staining for Podoplanin, a widely accepted marker of LVs[2]. Normal colonic biopsies showed sporadic thin LVs in the lamina propria and the submucosa, whereas CRC tissues both from non-metastatic (NM-) and metastatic (NM+) patients contained numerous LVs (Figure 1 A). Importantly, LVs within NM+ tumoral sections were loaded with metastatic cells (Figure 1 A, black arrows). Quantitative analysis revealed that LV density was significantly higher both in NM- and NM+ CRC patients, when compared to healthy tissue (Figure 1 B), with no differences between NM- and NM+ subjects, thus revealing that lymphangiogenesis occurs in human CRC independently from the metastatic process.

To verify the involvement of VEGFC/VEGFR3 pathway in metastatic CRC-associated lymphangiogenesis, human healthy and malignant CRC biopsies were analyzed for the expression of these two molecules, by Real-Time PCR, Western blot and immunofluorescence. Figure 1 C showed that VEGFC-expression levels were up-regulated in mucosal extracts of CRC patients, when compared to control tissues, while the other VEGFR3 ligand, VEGFD didn't change. This is in accordance with other studies, showing reduced levels of VEGFD in metastatic CRC[8]; for this reason the role of this specific growth factor was not taken into consideration for this study. Notably, VEGFR3-expression levels were up-regulated in mucosal extracts from CRC patients, when compared to healthy counterparts (Figure 1 D). Moreover, frozen-sections were double-stained for LYVE-1 and VEGFR3 (Figure 1 E) and their mean of fluorescence intensity (MFI) quantified, as recently described[22]. A lymphatic specific increase of VEGFR3 (Figure 1 F, left panel) but not LYVE-1 (Figure 1F, right panel) in CRC sections was observed compared to control tissues, indicating that the tumor microenvironment increases VEGFR3 expression on individual LVs. Collectively, these data

demonstrate that lymphatic vascularization is increased in human metastatic CRC, and suggest that the tumor microenvironment stimulates the VEGFC/VEGFR3 pathway on LVs, rather than VEGFD/VEGFR3 pathway, a finding compatible with tumor-induced lymphangiogenesis.

The VEGFC/VEGFR3 pathway is actively involved in the metastatic process of a CRC orthotopic model

In several cancer animal models, VEGFC has been found to enhance the passage of metastasis through LVs[13, 23]. To evaluate the functional role of the VEGFC/VEGFR3 pathway in metastatic CRC we modulated these two proteins in a well-known CRC mouse model[20]. Mice that underwent mCherry-positive CT26 cell orthotopic injection in the rectal mucosa were injected with an adenovirus encoding hVEGFC or with an anti-VEGFR3 antibody (mF431C1). Western blot and immunoprecipitation analyses of tissue lysates obtained from the colons of each experimental group clearly showed the efficient inhibition of VEGFR3 phosphorylation (Supplementary Figure 1 A, left panel) and upregulation of hVEGFC (Supplementary Figure 1 A, right panel) at the indicated time points. At 19 days of treatment lymphnodes (LNs), lungs and livers were processed for metastasis evaluation by FACS analysis (Figure 2, A and B). Quantification of mCherry-positive cells showed that systemic delivery of VEGFC significantly increased metastasis dissemination to draining LNs, lungs and livers (Figure 2 B). On the contrary, mF431C1 completely ablated CT26 migration to LNs, with only few cells detected in lungs and liver (Figure 2 B). Notably, the effect observed on metastasis was independent from primary tumor growth (Figure 2 C) and was unaltered by the effects of the VEGFC/VEGFR3 signaling pathway on CT26 biological functions (Figure 2, D and E). In fact, tumor size was unaltered upon VEGFC or mF431C1 treatment (Figure 2 C), and *in vitro* CT26 cells stimulated with VEGFC and/or VEGFR3 inhibitor, did not show any differences in both cell growth (Figure 2 D) and invasion (Figure 2 E). Moreover, CT26 cells did not express VEGFR2, VEGFR3 or VEGFC, as revealed by Real-time PCR analysis (Figure 2 F), thus confirming that the CT26-related metastatic process was not due to a direct effect of the VEGFC/VEGFR3 pathway on cancer cell proliferation and invasion.

We then evaluated whether the hastened VEGFC/VEGFR3-dependent metastatic dissemination correlated with altered lymphangiogenesis. For this purpose colons from CRC-bearing mice treated with VEGFC or mF431C1 were evaluated for LV expansion both in terms of LV density and size. Untreated tumor bearing mice (CT26) displayed increased LVs density (Figure 3, A and B) and size (Figure 3, D and E), when compared to control tumor-free animals (WT). Systemic delivery of the pro-lymphangiogenic factor VEGFC resulted in increased LV density (Figure 3, A and B) and dimension

(Figure 3, D and E), compared to untreated tumor-bearing mice. On the contrary, mF431C1 administered animals, displayed impaired lymphangiogeneis; in fact only few and small LVs were visible compared to untreated tumor bearing mice (Figure 3). Notably, the systemic delivery of VEGFC or VEGFR3 blocking antibody affected only LYVE-1 positive vessels, while these treatments did not alter the number (Figure 3 A and C) and dimensions (Figure 3, D and E) of CD31+ blood vessels, indicating that the VEGFC/VEGFR3 pathway has no impact on angiogenesis in our CRC model. Moreover, to exclude a possible influence of VEGFC and the virus itself on blood endothelial cells, Human Intestinal Blood Endothelial Cells (HIBECs) were efficiently infected with the same adenoviruses used *in vivo* (Supplementary Figure 1 B). Results showed that HIBECs proliferation (Supplementary figure 1 C), migration (Supplementary figure 1 D) and tubulogenesis (Supplementary figure 1 E) were affected neither by the virus itself nor by VEGFC released in the culture medium upon infection. Overall, these data demonstrate that VEGFR3 signaling is crucial for CRC progression through the lymphatic system, which correlates with the modulation of lymphangiogenesis at the tumor site.

The adherens junction protein VE-Cad is modulated during CRC metastasis on LVs in a VEGFC/VEGFR3-dependent manner

Although many efforts have been made to elucidate the role of VE-Cad expressed on blood vessels during cancer progression, little is known about its expression on LVs during tumor invasion, and no published data exists regarding its potential link to CRC. We hypothesized that VEGFR3 activation by VEGFC could lead to VE-Cad internalization on the lymphatic vasculature. To verify our hypothesis, tumor-bearing mice receiving AdVEGFC or mF431C1 treatment were evaluated for VE-Cad expression and distribution on colonic LVs. Results revealed that untreated tumor-bearing mice (CT26 group) had a discontinuous VE-Cad distribution on LVs, compared to control animals (WT group), which displayed the canonical button-like and zipper-like junctions[24] (Figure 4 A). Interestingly, alteration of VE-Cad expression on LVs was even more evident in AdVEGFC treated mice, while upon VEGFR3 blocking, was observed a partial restoration of VE-Cad distribution on LVs, compared to healthy animals (Figure 4 A). Frozen sections of colons derived from each experimental group, were stained for LYVE-1 and VE-Cad (Figure 4 B) and MFI was calculated. Quantification analysis in Figure 4 C demonstrated that while untreated tumor-bearing mice displayed a significant reduction in VE-Cad MFI compared to healthy controls, systemic delivery of VEGFC significantly decreased VE-Cad expression, when compared to the CT26 only group. On the contrary, mice treated with mF314C1 had an increased expression of VE-Cad on LYVE-1-positive vessels, comparable to healthy controls

(Figure 4 C). Importantly, similar results were obtained in VEGFC- or mF431C1-treated healthy mice (Supplementary Figure 1 F), indicating that the VEGFC/VEGFR3 pathway is actively involved in regulating VE-Cad expression and distribution on intestinal LVs both in physiological conditions and during metastatic CRC.

Modulation of VEGFR3 signaling leads to VE-Cad internalization and β-catenin cytoplasmic release in HILEC

To directly study the link between VE-Cad and VEGFR3 signaling in intestinal LVs, we isolated and functionally characterized Human Intestinal Lymphatic Endothelial Cells (HILEC)[22]. For this purpose, HILECs were stimulated with VEGFC and/or with SAR131675 (SAR), a tyrosine kinase inhibitor that specifically targets VEGFR3[25]. Cells were stained for the lymphatic marker Prox-1 and VE-Cad, and cell membrane VE-Cad MFI was quantified. Stimulation with VEGFC increased cytoplasmic VE-Cad localization (Figure 5 A, white arrows), when compared to unstimulated cells (UN) and altered VE-Cad distribution on HILEC's cell membrane (Figure 5 A, red arrows), resulting in a discontinuous expression pattern of this adherens junction molecule, and a reduced membrane MFI (Figure 5 B). The VEGFC-dependent effects were abolished by inhibition of VEGFR3 (Figure 5, A and B). HILECs treated only with SAR displayed similar cell membrane VE-Cad localization and MFI, in comparison with UN cells, with no internalization of the protein (Figure 5, A and B). These findings show that VE-Cad distribution and internalization directly depends on VEGFR3 activation by VEGFC, as observed *in vivo* (Figure 4).

Since in quiescent cells, β-catenin interacts with VE-Cad in complexes mainly at the plasma membrane, maintaining a low level of β-catenin at the cytoplasm[16], we stained HILECs also for this protein (Figure 5 A). VEGFC-treated cells displayed a reduction in β-catenin at the plasma-membrane compared to unstimulated HILECs. In the presence of SAR the effects of VEGFC on β-catenin membrane localization were lost (Figure 5 A). We therefore measured β-catenin cell membrane MFI. Notably, HILECs treated with SAR alone did not display a significant increase in β-catenin, when compared with untreated cells. VEGFC-stimulated cells had a lower plasma-membrane β-catenin MFI compared to untreated controls, whereas SAR abolished these effects (Figure 5 C). MFI of β-catenin in cells treated with the VEGFR3 inhibitor alone was comparable to that of untreated cells. Importantly, HIBECs infected with AdVEGFC displayed comparable distribution and internalization of both VE-Cad and β-catenin (Supplementary Figure 2 A) indicating that VEGFC has a direct effect only on LECs.

Taken together, these results suggest that VEGFC-dependent VEGFR3 activation impairs cell-cell adhesion by inducing the disassembly of the VE-Cad-β-catenin complex at intercellular junctions.

VEGFR3 activation by VEGFC alters HILEC permeability and affects CT26 cell transdentothelial migration

Cell-cell adherens junctions are important for endothelial barrier function and integrity[16]. For this reason, we assessed the capability of the VEGFC/VEGFR3 signaling pathway to modulate HILECs permeability through induction of intercellular junction opening. HILECs were stimulated with VEGFC and/or SAR and permeability was assessed by measuring the trans-endothelial electrical resistance (TEER). VEGFC-treated HILECs showed a significant decrease in TEER across the cell monolayer, when compared to unstimulated cells (Figure 6 A). This effect was abolished by SAR, resembling untreated control cells. Notably, SAR-treated HILECs displayed the same TEER as untreated cells, demonstrating the specific dependence of intestinal lymphatic endothelial cell permeability on VEGFC/VEGFR3 activation.

To mimic the cancer cell intravasation/extravasation process *in vitro*, we performed a transendothelial migration assay using a co-culture of HILECs and mCherry CT26 cells (Figure 6 B). HILECs were treated with VEGFC and/or SAR, and mCherry CT26 transendothelial migration was quantified after 16 hours of co-culture. Results showed that VEGFC induced an increase in CT26 migration, when compared to untreated HILEC. Interestingly, treatment with both VEGFC and the VEGFR3 inhibitor showed similar CT26 migration, in comparison to untreated controls (Figure 6, C and D). Moreover, HILECs treated with SAR alone displayed a slight reduction in CT26 transmigration (Figure 6, C and D), revealing a direct effect of VEGFC-dependent-VEGFR3 activation on CRC cell transendothelial migration. Notably, AdVEGFC has no effect on CT26 trasendothelial migration through HIBECs (Supplementary Figure 2 B), indicating that VEGFC doesn't play a role in hematogenous metastatic spread.

LVs in tumor tissue of metastatic CRC patients displayed decreased VE-Cad levels

To confirm what was observed *in vivo* and *in vitro*, we further evaluated VE-Cad expression levels on LYVE-1+ vessels in metastatic CRC patients, and compared them with controls. Normal colon tissues showed a strong expression of VE-Cad on LVs, whereas CRC sections had a significant cadherin decrease (Figure 7 A). Co-expression of VE-Cad and LYVE-1 was quantified revealing a lymphatic specific decrease of this cadherin in CRC sections compared with controls (Figure 7 B). This result correlated with high levels of both VEGFC and VEGFR3 in the CRC microenvironment. Overall, these data demonstrate that lymphatic vascularization is increased in CRC tissues, and that the tumor

microenvironment stimulates the VEGFC/VEGFR3 pathway, in association with decreased VE-Cad on LVs. These elements contribute to an impaired lymphatic endothelial barrier function and facilitate lymphatic metastatic spread, as described in Figure 7 C. Stimulation of VEGFC leads to the induction of VEGFR3 signaling causing VE-Cad-β-catenin dissociation, VE-Cad internalization and β-catenin cytoplasmic release resulting in cell-junction opening and increased metastatic spread (Figure 7 C).

Discussion

Tumor induced-angiogenesis and lymphangiogenesis are thought to expedite cancer cell entry into the blood and lymphatic vasculature, thus fostering metastatic dissemination[14]. However, while the role of the vascular endothelium in cancer progression is well described[26], the contribution of tumoral LVs is still unclear. In many types of human cancers, including CRC[3-5], the expression of VEGFC[2] and its receptor, VEGFR3[25, 27], correlates with lymphangiogenic sprouting, metastases and poor prognosis. In accordance with these studies, we confirmed that active lymphangiogenesis takes place in CRC patients displaying a high expression of VEGFC and increased VEGFR3 levels on LVs. VEGFD is also known to be a VEGFR3 ligand and is considered an important pro-lymphangiogenic factor[28]; however, unlike VEGFC, it was not altered in CRC patients, and for this reason our study only focused on VEGFC. Several cancer animal models have highlighted the importance of the lymphatic vasculature in metastatic dissemination thanks to the modulation of the VEGFC/VEGFR3 pathway. In fact, He et al. demonstrated in a mouse model of lung cancer, that VEGFC-overexpressing LNM35 cells induce massive lymphangiogenesis together with lymphatic activation, thus facilitating tumor cell entry in LVs and promoting metastatic dissemination to LNs[14]. Notably, in this study LV destabilization and tumor metastases were blocked using an Adenovirus producing a soluble VEGFR3-Ig fusion protein[14]. Moreover, Matsumoto et al. showed that in a mouse model of breast cancer, VEGFR3 signaling was required for the early events of the metastatic process and that mF431C1 was able to block both tumor lymphangiogenesis and metastases[27]. In a similar way, our study shows that LVs undergo dramatic lymphangiogenic changes in response to nearby CT26 mCherry cells, including sprouting and dilation of the larger collecting vessels draining the tumor area. We demonstrate for the first time that upon VEGFR3 inhibition, tumor-lymphangiogenesis represents a rate-limiting step for CRC lymphogenous metastases, which are significantly suppressed at distant organs. In contrast, upon systemic VEGFC delivery, metastasis is fostered in association with active lymphangiogenesis. Consistent with other findings, in the tumoral context we do not observe any effects on blood vessel density and enlargement upon VEGFC treatment[29, 30] or VEGFR3 inhibition[7]. It is worthy of note that these experiments do not

exclude the possibility that VEGFC could act on other cells other than lymphatic endothelial cells, such as VEGFR3-expressing macrophages[25].

It is still unclear whether tumor cell intravasation/extravasation requires the transmigration of cancer cells through the cytoplasm of endothelial cells, as occurs for leukocytes, or whether they transmigrate between two adjacent endothelial cells after the disruption of cell-cell connections[19]. The endothelial barrier integrity is maintained by a complex balance between cell-to-cell adherens junctions. In some pathological conditions, such as inflammation and cancer, endothelial junctions can be disrupted leading to the opening of intercellular gaps and inducing increased vascular permeability[31]. We focused our attention on the most important player in maintaining barrier integrity: VE-Cad. In fact, blocking VE-Cad is sufficient to destabilize endothelial cell contacts *in vivo* and to increase vascular permeability[32]. In contrast, stabilizing endothelial cell junctions by enhancing the VE-Cad adhesive function in knock-in mice leads to the induction of vascular permeability and leukocyte extravasation[3, 33]. One of the mechanisms involved in adherens junction destabilization is the activation of VEGFR2 by VEGFA which induces VE-Cad tyrosine phosphorylation and its internalization[16]. In this scenario, VEGFA facilitates cancer cell intravasation by disrupting the VE-Cad-β-catenin complex and inducing adherens junction weakness and formation of transcellular holes[34]. Weis et al., provided evidence that VEGFA-mediated breakdown in blood endothelial integrity through VE-Cad disruption hastens metastases[19]. Moreover, they demonstrated that VE-Cad inhibition compromises endothelial barrier function and promotes tumor cell extravasation[19]. We hypothesized that similarly to blood vessels, the lymphatic vasculature could respond to the modulation of the VEGFC/VEGFR3 pathway with VE-Cad redistribution. *In vitro* results on HILEC confirmed our hypothesis; in fact, VEGFC-induced VEGFR3 signaling led to VE-Cad-β-catenin complex dissociation, VE-Cad internalization and β-catenin cytoplasmic release. Breslin et al. demonstrated that VEGFC-dependent VEGFR3 activation significantly increased lymphatic endothelial cell permeability[35]. In accordance with the above study, we provide *in vivo* evidence that VEGFR3 signaling induces major alterations in the intestinal lymphatic barrier and strongly impairs its functionality. Importantly, we propose a mechanism of CRC cell intravasation/extravasation that is dependent on VEGFR3 activation on lymphatic endothelial cells which facilitates tumor cell entry/exit in a VEGFC-dependent manner. The most intriguing and novel finding of our study is that the increased metastasis formation in VEGFC-treated mice during CRC progression is not only a consequence of enhanced lymphangiogenesis, but could also be a result of VE-Cad distribution and localization on LVs. In fact, VEGFC stimulates LVs sprouting and dilation, but also modulates VE-Cad expression on intestinal lymphatics. These results are in accordance with

Tammela et al. who observed that VEGFC delivery induces VE-Cad downregulation on lymphatic capillaries[36]. Interestingly, upon VEGFR3 inhibition VE-Cad localization in tumor-bearing mice was comparable to healthy animals, thus directly linking VE-Cad distribution with the VEGFC/VEGFR3 pathway and lymphogenous metastases. These findings confirm our *in vitro* data and are consistent with what we observed in human metastatic CRC specimens. As in the mouse, human CRC samples have consistent overexpression of VEGFC and VEGFR3 in tumor tissue which overlaps with increased lymphangiogenesis and diminished lymphatic VE-Cad expression. At present, the lymphatic route of tumor metastases is less understood compared to the vascular route[37]. Our results help to better understand metastatic dissemination through lymphatics; however, they do not exclude that other molecules released in the tumor microenvironment could be involved in lymphatic barrier alteration, such as some inflammatory mediators[38].

LVs are largely quiescent in adults[39], thus lymphangiogenesis may provide a safe target for cancer metastases. The use of neutralizing antibodies targeting VEGFC and/or VEGFR3 in clinical studies which have progressed to Phase I clinical trials in patients with advanced solid tumors[15] have provided encouraging results. Furthermore, several small-molecule protein kinase inhibitors (PKIs) targeting various kinases, including VEGFR3, are now available and some of them have been approved for the treatment of various cancers[15], showing an overall survival benefit in patients with refractory metastatic CRC[40].

In summary, our findings strongly support and encourage a VEGFC/VEGFR3-targeted therapy for the prevention of CRC metastatic dissemination. The inhibition of this signaling pathway may reduce tumor lymphangiogenesis and restore lymphatic barrier integrity through the maintenance of VE-Cad distribution on LVs. The lymphatic vasculature may thus represent a potent target to abate and prevent CRC lymphogenous spread.

Figure legends:

Figure 1. **Lymphatic vessel density, VEGFC and VEGFR3 signaling are increased in the colon of CRC patients**

(**A, B**) Immunohistochemical staining with an antibody recognizing Podoplanin was performed on healthy (NL, n=15), non-metastatic (NM-, n=13) or metastatic (NM+, n=13) CRC colon tissues (**A**), and quantitative analysis of LV density is shown in (**B**). Data are expressed as mean percentage of LV per area ±SD. Bar: 100 µm. **P<0,01, ***P<0,001 by ANOVA test with Bonferroni's correction for multiple comparisons. (**C, D**) Healthy (NL, n=13) and metastatic CRC (NM+, n=13) patients were

measured for VEGFC and VEGFR3 content in mucosal extracts, by Real-time PCR (**C**) and Western blot analysis (**D**), respectively. (**E**) Representative images of frozen-sections from the colon of control (NL, n=8) or metastatic CRC (NM+, n=8) patients stained for LYVE-1 (red), VEGFR3 (green) and DAPI (blue). Bar: 100 µm. (**F**) The mean fluorescence intensity (FI) per vessel was analyzed on VEGFR3+ (left panel) and LYVE-1+ (right panel) LVs (10-15 vessels/patient). FI are relative units normalized per vascular area expressed in square micrometers. Values are mean ±SD. *P<0,05, **P<0,01 vs. NL by Student's t-test. M= mucosa, LP= lamina propria, MM=mucolaris mucosae; SM= submucosa.

Figure 2. VEGFC/VEGFR3 pathway activation increases metastatic dissemination of CRC without targeting CT26 cells

Mice receiving mCherry CT26 ortothopic injection were administered with an adenovirus encoding hVEGFC, or anti-VEGFR3 antibody (mF431C1). (**A**, **B**) FACS analysis shows mCherry-positive cells in the liver, lung and LNs. (**C**) Tumor growth and dimension were measured by IVIS *in vivo* imaging system (left panel) and caliper (right panel). Results are expressed as mean tumor volume (mm^3) vs. untreated (CT26) of three independent experiments (n= 6 mice/group). (**D**) CT26 cell proliferation was quantified by crystal violet and data are expressed as 560 nm absorbance. Values are mean ± SD of three independent experiments with six replicates per group. (**E**) CT26 cells were subjected to migration through matrigel-coated filters for 16 hours and the number of migrated cells vs. UN per filter was reported. (**F**) Confluent CT26 cells were examined for the expression of VEGFR3, VEGFR2 and VEGFC by Real-time PCR and were compared to healthy mouse colons (Ctrl tissue). Values are means ± SD of three independent experiments with three replicates/group. *P<0,05; **P<0,01 vs. control (CT26) by ANOVA test with Dunnet's correction for multiple comparisons.

Figure 3. The activation of VEGFR3 signaling fosters lymphangiogenesis in CRC

(**A**) Representative images of frozen-sections from colons of animals without tumor (WT) and CT26 bearing mice, with or without adenoviruses encoding hVEGFC, or anti-VEGFR3 antibody (mF431C1). Tissues were stained for LYVE-1 (green), CD31 (red) and DAPI (blue), and LYVE-1+ (**B**) and CD31+LYVE1- (**C**) vessels were counted in 10 comparable regions per section. Results are expressed as mean values ± SD, and are representative of three independent experiments (n=3 mice/group). Scale bar: 100 µm. (**D, E**) Whole mounts of distal colonic segments from the indicated experimental groups were stained for LYVE-1 (green) and CD31 (red). (**D**) Representative images of whole mount staining of distal colons from the indicated groups. (**E**) LV and blood vessels diameters were quantified and reported as mean values ± SD of three independent experiments, (n=3 mice/group with 5 fields/colonic

segment for each experiment). Scale bar 200 µm. ***P<0,001; vs CT26 by ANOVA test with Dunnet's correction for multiple comparisons.

Figure 4. **Systemic delivery of human VEGFC alters VE-Cad pattern distribution and expression on LVs**

(**A**) Representative images of whole mount tissues from colons of animals without tumor (WT) and CT26 bearing mice, with or without AdVEGFC, or mF431C1 and stained for LYVE-1 (green) and VE-Cad (red). Lower panels are higher magnifications of the white dashed squares in the upper panel. Scale bar: 50µm. (**B**, **C**) Frozen-sections from the colon of all experimental groups were stained with both anti-LYVE-1 and anti-VE-Cad antibodies, with representative images expressed in (**B**). VE-Cad mean FI per vessel was analyzed on LYVE-1+ vessels, and FI is expressed in (**C**) as relative units per vascular area. Scale bar: 20µm. Results are representative of three independent experiments with three mice per group. Values are expressed as Mean ±SD. *P<0,05, **P<0,01; vs. CT26 by ANOVA test with Dunnet's correction for multiple comparisons.

Figure 5. Modulation of the VEGFR3 signaling pathway mediates VE-Cad and β-catenin internalization on HILEC

(**A**) Representative merges of HILECs stained for the lymphatic marker Prox-1 (magenta), DAPI (blue), β-catenin (red) and VE-Cad (green). Cells were left untreated (UN), stimulated for 30 min with VEGFC, in the presence or absence of the VEGFR3 inhibitor SAR131675 (SAR). Representative merges of HILECs stained for Prox-1 (magenta), DAPI (blue), β-catenin (red) and VE-Cad (green). VEGFC stimulation induced VE-Cad internalization (white arrows) along with a discontinuous VE-Cad membrane distribution (red arrows). (**B, C**) Cell surface mean FI was analyzed for VE-Cad (**B**) and β-catenin (**C**). Results are representative of three independent experiments each in triplicate/group. Scale bar: 50 µm. Values are expressed as Mean ±SD. *P<0,05; vs. UN by ANOVA test with Dunnet's correction for multiple comparisons.

Figure 6. **VEGFR3 activation by VEGFC alters HILEC permeability and modulates CT26 cell transdentothelial migration**

(**A**) HILECs permeability was quantified through TEER. Inhibition of VEGFR3 was achieved by adding SAR131675 (SAR) (23 µM) 30 min prior to VEGFC (100 ng/ml). Bars represent mean values per group ±SD. Bar: 50 µm. *P<0,05; **P<0,01 vs. UN by ANOVA test with Dunnet's correction for multiple comparisons. (**B)** Cartoon of the transendothelial migration assay: mCherry-CT26 cells were seeded on HILEC confluent monolayers left untreated (UN), treated with VEGFC and/or with SAR131675, VEGFC+SAR and SAR alone, respectively. MCherry-positive transmigrated cells were

counted (**D**) and representative images are shown in (**C)**. Data are expressed as mean ± SD of 3 experiments performed in triplicate. Magnification: 10x. ***P<0,001; vs. UN by ANOVA test with Dunnet's correction for multiple comparisons.

Figure 7. V**E-Cad expression is decreased on LVs of metastatic CRC patients**

(**A, B**) Representative frozen-sections from the colon of control (NL) (n=8) or metastatic CRC (NM+) (n=8) patients were stained for both LYVE-1 and VE-Cad (**A**). Bar: 100µm. (**B**) VE-Cad mean fluorescence intensity (FI) per vessel was analyzed on LYVE-1+ LVs. FI is expressed as relative units per vascular area (10-15 vessels/patient). Values are expressed as Mean ± SD. *P<0,05; vs. NL by Student's t-test. **(C)** The left panel shows that under physiological conditions, intestinal lymphatic endothelial cells (ILECs) are quiescent and the barrier integrity is maintained. In the central panel, VEGFC secreted in the tumor microenvironment stimulates VEGFR3 overexpressed on ILECs and impairs endothelial barrier integrity, thus promoting lymphogenous metastasis formation. In the right panel, inhibition of VEGFR3 signaling maintains lymphatic barrier functionality and abates metastasis dissemination.

References

1. Schoppmann A, Tamandl D, Herberger B, et al. Comparison of lymphangiogenesis between primary colorectal cancer and corresponding liver metastases. Anticancer Res 2011;31:4605-11.
2. **Li X, Liu B**, Xiao J, et al. Roles of VEGF-C and Smad4 in the lymphangiogenesis, lymphatic metastasis, and prognosis in colon cancer. J Gastrointest Surg 2011;15:2001-10.
3. Broermann A, Winderlich M, Block H, et al. Dissociation of VE-PTP from VE-cadherin is required for leukocyte extravasation and for VEGF-induced vascular permeability in vivo. J Exp Med 2011;208:2393-401.
4. Garouniatis A, Zizi-Sermpetzoglou A, Rizos S, et al. Vascular endothelial growth factor receptors 1,3 and caveolin-1 are implicated in colorectal cancer aggressiveness and prognosis--correlations with epidermal growth factor receptor, CD44v6, focal adhesion kinase, and c-Met. Tumour Biol 2013;34:2109-17.
5. Royston D, Jackson DG. Mechanisms of lymphatic metastasis in human colorectal adenocarcinoma. J Pathol 2009;217:608-19.
6. Wang Y, Oliver G. Current views on the function of the lymphatic vasculature in health and disease. Genes Dev 2010;24:2115-26.
7. Pytowski B, Goldman J, Persaud K, et al. Complete and specific inhibition of adult lymphatic regeneration by a novel VEGFR-3 neutralizing antibody. J Natl Cancer Inst 2005;97:14-21.
8. George ML, Tutton MG, Janssen F, et al. VEGF-A, VEGF-C, and VEGF-D in colorectal cancer progression. Neoplasia 2001;3:420-7.

9. Shibuya M, Claesson-Welsh L. Signal transduction by VEGF receptors in regulation of angiogenesis and lymphangiogenesis. Exp Cell Res 2006;312:549-60.
10. Tammela T, Alitalo K. Lymphangiogenesis: Molecular mechanisms and future promise. Cell 2010;140:460-76.
11. Steeg PS. Tumor metastasis: mechanistic insights and clinical challenges. Nat Med 2006;12:895-904.
12. Mandriota SJ, Jussila L, Jeltsch M, et al. Vascular endothelial growth factor-C-mediated lymphangiogenesis promotes tumour metastasis. EMBO J 2001;20:672-82.
13. Skobe M, Hawighorst T, Jackson DG, et al. Induction of tumor lymphangiogenesis by VEGF-C promotes breast cancer metastasis. Nat Med 2001;7:192-8.
14. He Y, Rajantie I, Pajusola K, et al. Vascular endothelial cell growth factor receptor 3-mediated activation of lymphatic endothelium is crucial for tumor cell entry and spread via lymphatic vessels. Cancer Res 2005;65:4739-46.
15. Stacker SA, Williams SP, Karnezis T, et al. Lymphangiogenesis and lymphatic vessel remodelling in cancer. Nat Rev Cancer 2014;14:159-72.
16. Dejana E, Orsenigo F, Lampugnani MG. The role of adherens junctions and VE-cadherin in the control of vascular permeability. J Cell Sci 2008;121:2115-22.
17. Leckband D, Sivasankar S. Mechanism of homophilic cadherin adhesion. Curr Opin Cell Biol 2000;12:587-92.
18. Lampugnani MG, Corada M, Caveda L, et al. The molecular organization of endothelial cell to cell junctions: differential association of plakoglobin, beta-catenin, and alpha-catenin with vascular endothelial cadherin (VE-cadherin). J Cell Biol 1995;129:203-17.
19. Weis S, Cui J, Barnes L, et al. Endothelial barrier disruption by VEGF-mediated Src activity potentiates tumor cell extravasation and metastasis. J Cell Biol 2004;167:223-9.
20. Donigan M, Loh BD, Norcross LS, et al. A metastatic colon cancer model using nonoperative transanal rectal injection. Surg Endosc 2010;24:642-7.
21. Nagahashi M, Ramachandran S, Rashid OM, et al. Lymphangiogenesis: a new player in cancer progression. World J Gastroenterol 2010;16:4003-12.
22. D'Alessio S, Correale C, Tacconi C, et al. VEGF-C-dependent stimulation of lymphatic function ameliorates experimental inflammatory bowel disease. J Clin Invest 2014.
23. Karpanen T, Alitalo K. Lymphatic vessels as targets of tumor therapy? J Exp Med 2001;194:F37-42.
24. Baluk P, Fuxe J, Hashizume H, et al. Functionally specialized junctions between endothelial cells of lymphatic vessels. J Exp Med 2007;204:2349-62.
25. Alam A, Blanc I, Gueguen-Dorbes G, et al. SAR131675, a potent and selective VEGFR-3-TK inhibitor with antilymphangiogenic, antitumoral, and antimetastatic activities. Mol Cancer Ther 2012;11:1637-49.
26. Weis SM, Cheresh DA. Tumor angiogenesis: molecular pathways and therapeutic targets. Nat Med 2011;17:1359-70.
27. Matsumoto M, Roufail S, Inder R, et al. Signaling for lymphangiogenesis via VEGFR-3 is required for the early events of metastasis. Clin Exp Metastasis 2013;30:819-32.
28. Achen MG, Stacker SA. Vascular endothelial growth factor-D: signaling mechanisms, biology, and clinical relevance. Growth Factors 2012;30:283-96.
29. Liersch R, Hirakawa S, Berdel WE, et al. Induced lymphatic sinus hyperplasia in sentinel lymph nodes by VEGF-C as the earliest premetastatic indicator. Int J Oncol 2012;41:2073-8.

30. Saaristo A, Veikkola T, Enholm B, et al. Adenoviral VEGF-C overexpression induces blood vessel enlargement, tortuosity, and leakiness but no sprouting angiogenesis in the skin or mucous membranes. FASEB J 2002;16:1041-9.
31. Mierke CT. Role of the endothelium during tumor cell metastasis: is the endothelium a barrier or a promoter for cell invasion and metastasis? J Biophys 2008;2008:183516.
32. Corada M, Mariotti M, Thurston G, et al. Vascular endothelial-cadherin is an important determinant of microvascular integrity in vivo. Proc Natl Acad Sci U S A 1999;96:9815-20.
33. Schulte D, Kuppers V, Dartsch N, et al. Stabilizing the VE-cadherin-catenin complex blocks leukocyte extravasation and vascular permeability. EMBO J 2011;30:4157-70.
34. Folkman J. Angiogenesis. Annu Rev Med 2006;57:1-18.
35. Breslin JW, Yuan SY, Wu MH. VEGF-C alters barrier function of cultured lymphatic endothelial cells through a VEGFR-3-dependent mechanism. Lymphat Res Biol 2007;5:105-13.
36. Tammela T, Saaristo A, Holopainen T, et al. Therapeutic differentiation and maturation of lymphatic vessels after lymph node dissection and transplantation. Nat Med 2007;13:1458-66.
37. Nathanson SD. Insights into the mechanisms of lymph node metastasis. Cancer 2003;98:413-23.
38. Breslin JW. ROCK and cAMP promote lymphatic endothelial cell barrier integrity and modulate histamine and thrombin-induced barrier dysfunction. Lymphat Res Biol 2011;9:3-11.
39. Alitalo A, Detmar M. Interaction of tumor cells and lymphatic vessels in cancer progression. Oncogene 2012;31:4499-508.
40. Grothey A, Van Cutsem E, Sobrero A, et al. Regorafenib monotherapy for previously treated metastatic colorectal cancer (CORRECT): an international, multicentre, randomised, placebo-controlled, phase 3 trial. Lancet 2013;381:303-12.

Authors names in bold designate shared co-first authors

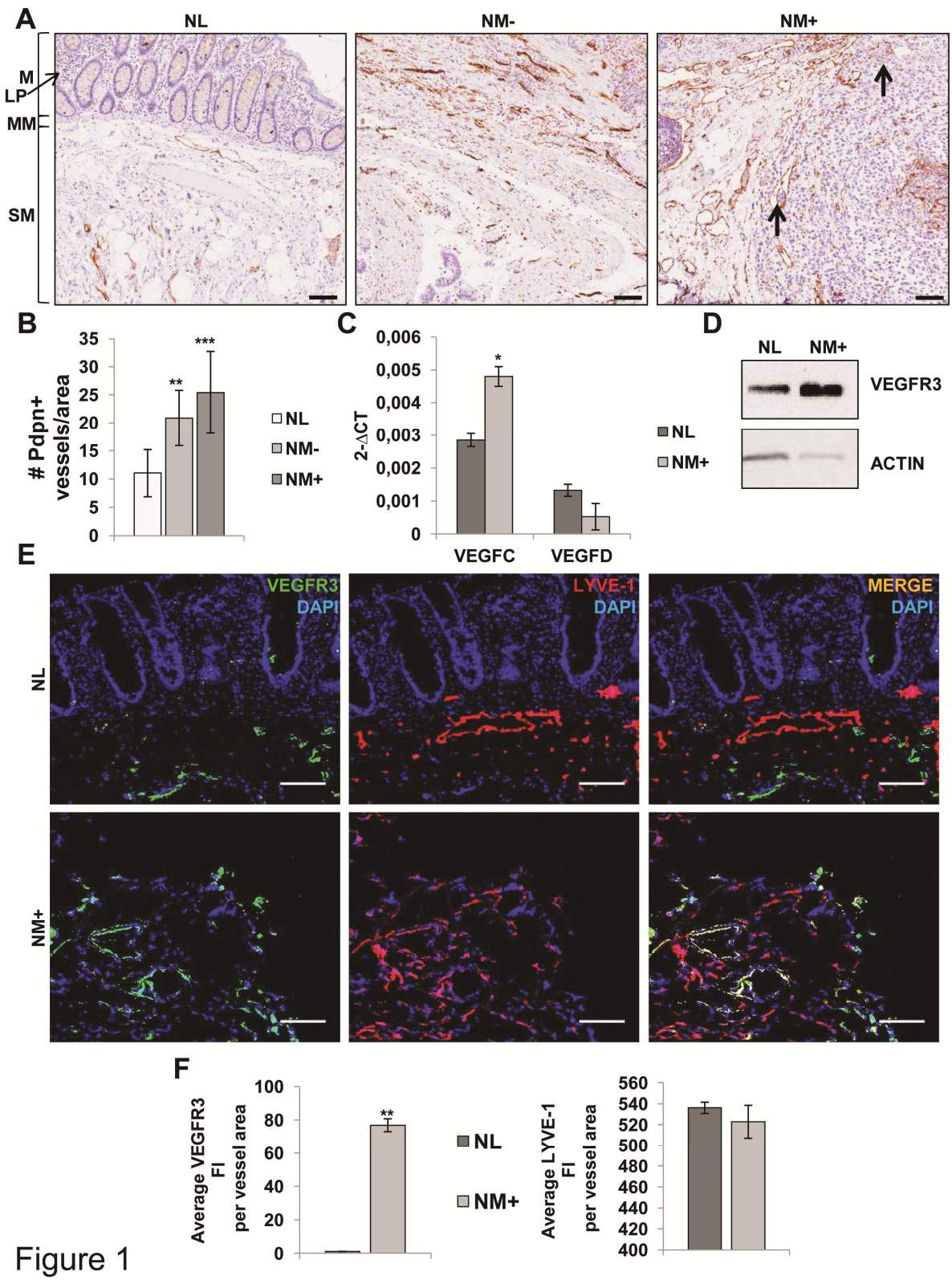
A
NL
NM-
NM+
M
LP
MM
SM
B
Pdpn+ vessels/area
35
30
25
20
15
10
5
0
**
***
NL
NM-
NM+
C
2-ΔCT
0,006
0,005
0,004
0,003
0,002
0,001
0
*
VEGFC
VEGFD
D
NL
NM+
VEGFR3
ACTIN
E
VEGFR3
DAPI
LYVE-1
DAPI
MERGE
DAPI
NL
NM+
F
Average VEGFR3 FI per vessel area
100
80
60
40
20
0
**
NL
NM+
Average LYVE-1 FI per vessel area
560
540
520
500
480
460
440
420
400

Figure 1

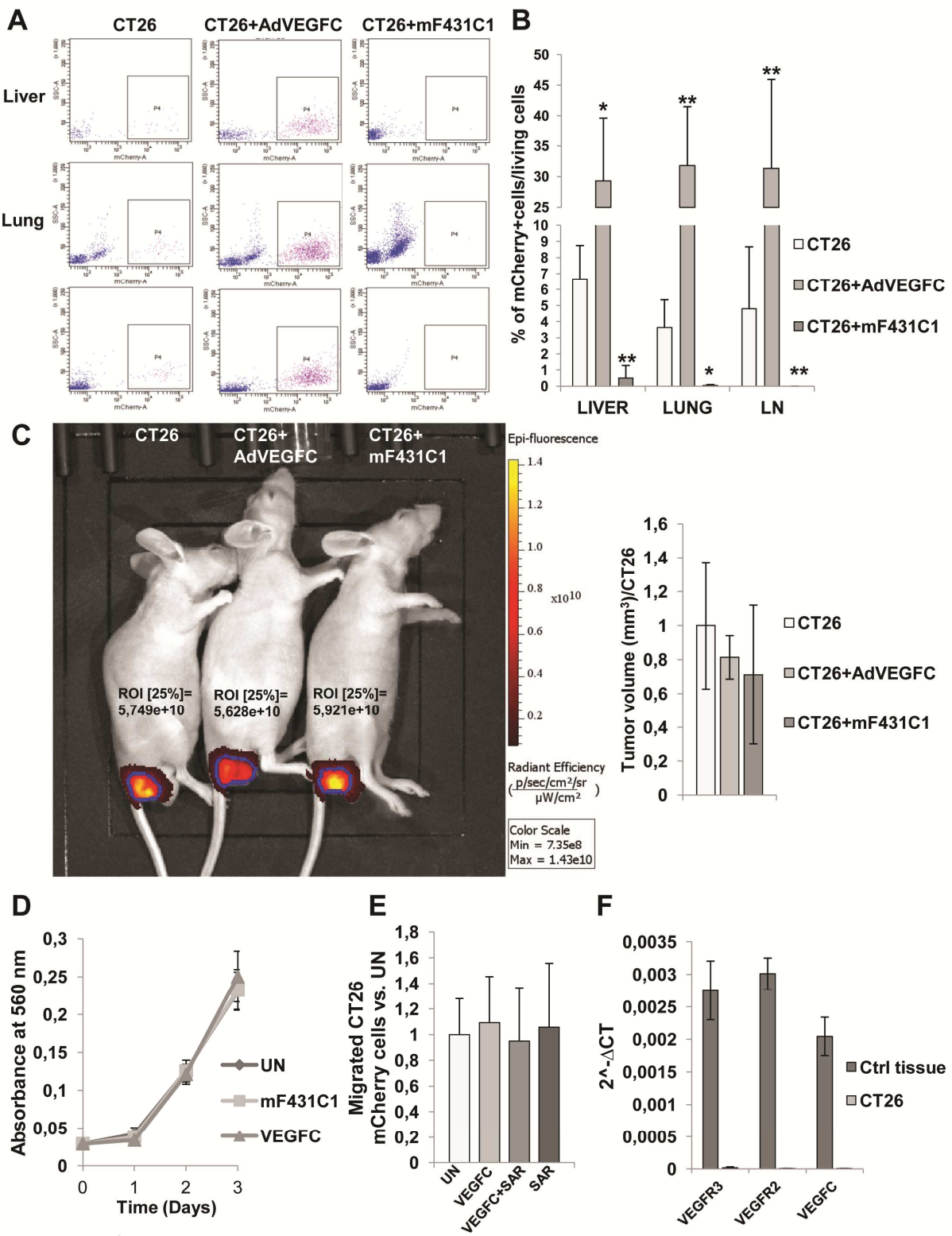
A
CT26
CT26+AdVEGFC
CT26+mF431C1
Liver
Lung
B
% of mCherry+cells/living cells
CT26
CT26+AdVEGFC
CT26+mF431C1
LIVER
LUNG
LN
C
CT26
CT26+ AdVEGFC
CT26+ mF431C1
ROI [25%]= 5,749e+10
ROI [25%]= 5,628e+10
ROI [25%]= 5,921e+10
Epi-fluorescence
x10^10
Radiant Efficiency
Color Scale
Min = 7.35e8
Max = 1.43e10
Tumor volume (mm3)/CT26
CT26
CT26+AdVEGFC
CT26+mF431C1
D
Absorbance at 560 nm
Time (Days)
UN
mF431C1
VEGFC
E
Migrated CT26 mCherry cells vs. UN
UN
VEGFC
VEGFC+SAR
SAR
F
2^-ΔCT
Ctrl tissue
CT26
VEGFR3
VEGFR2
VEGFC

Figure 2

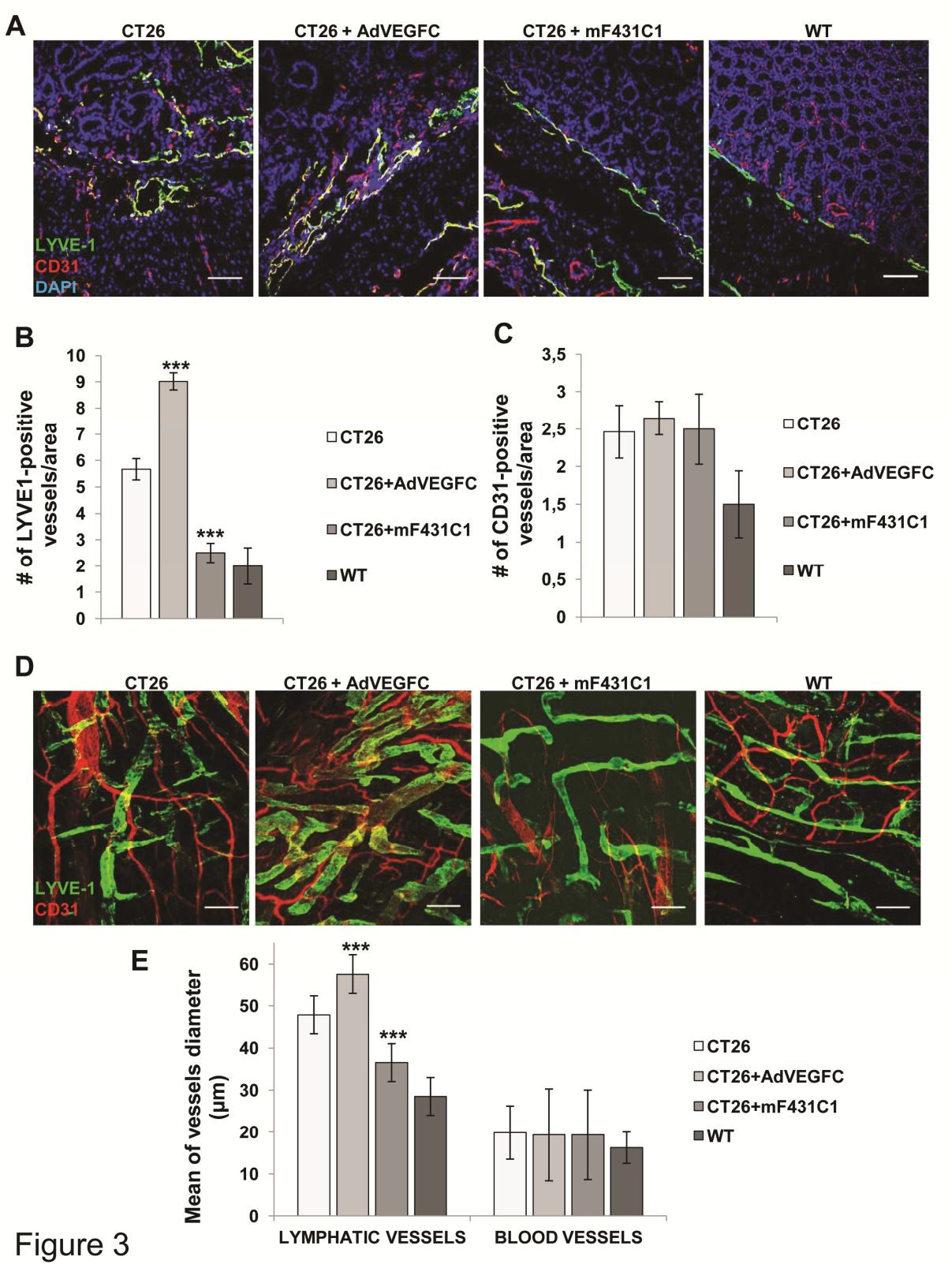
A
CT26
CT26 + AdVEGFC
CT26 + mF431C1
WT
LYVE-1
CD31
DAPI
B
# of LYVE1-positive vessels/area
***
***
CT26
CT26+AdVEGFC
CT26+mF431C1
WT
C
# of CD31-positive vessels/area
CT26
CT26+AdVEGFC
CT26+mF431C1
WT
D
CT26
CT26 + AdVEGFC
CT26 + mF431C1
WT
LYVE-1
CD31
E
Mean of vessels diameter (µm)
***
***
CT26
CT26+AdVEGFC
CT26+mF431C1
WT
LYMPHATIC VESSELS
BLOOD VESSELS

Figure 3

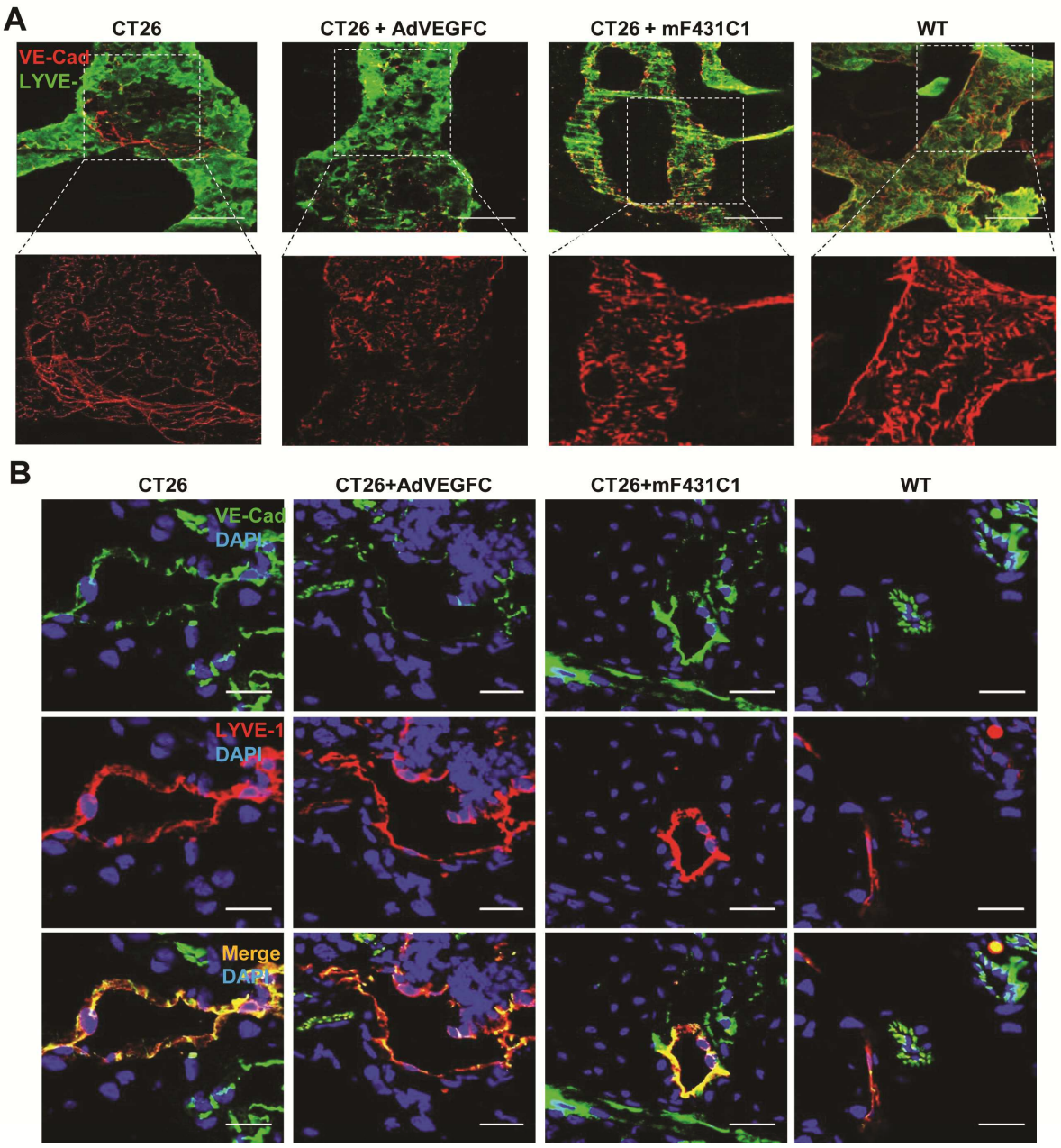
A
CT26
CT26 + AdVEGFC
CT26 + mF431C1
WT
VE-Cad
LYVE-1
B
CT26
CT26+AdVEGFC
CT26+mF431C1
WT
VE-Cad
DAPI
LYVE-1
DAPI
Merge
DAPI
C
Average VE-Cad FI per vessel area
1.200.000
1.000.000
800.000
600.000
400.000
200.000
0
*
**
CT26
CT26+AdVEGFC
CT26+mF431C1
WT

Figure 4

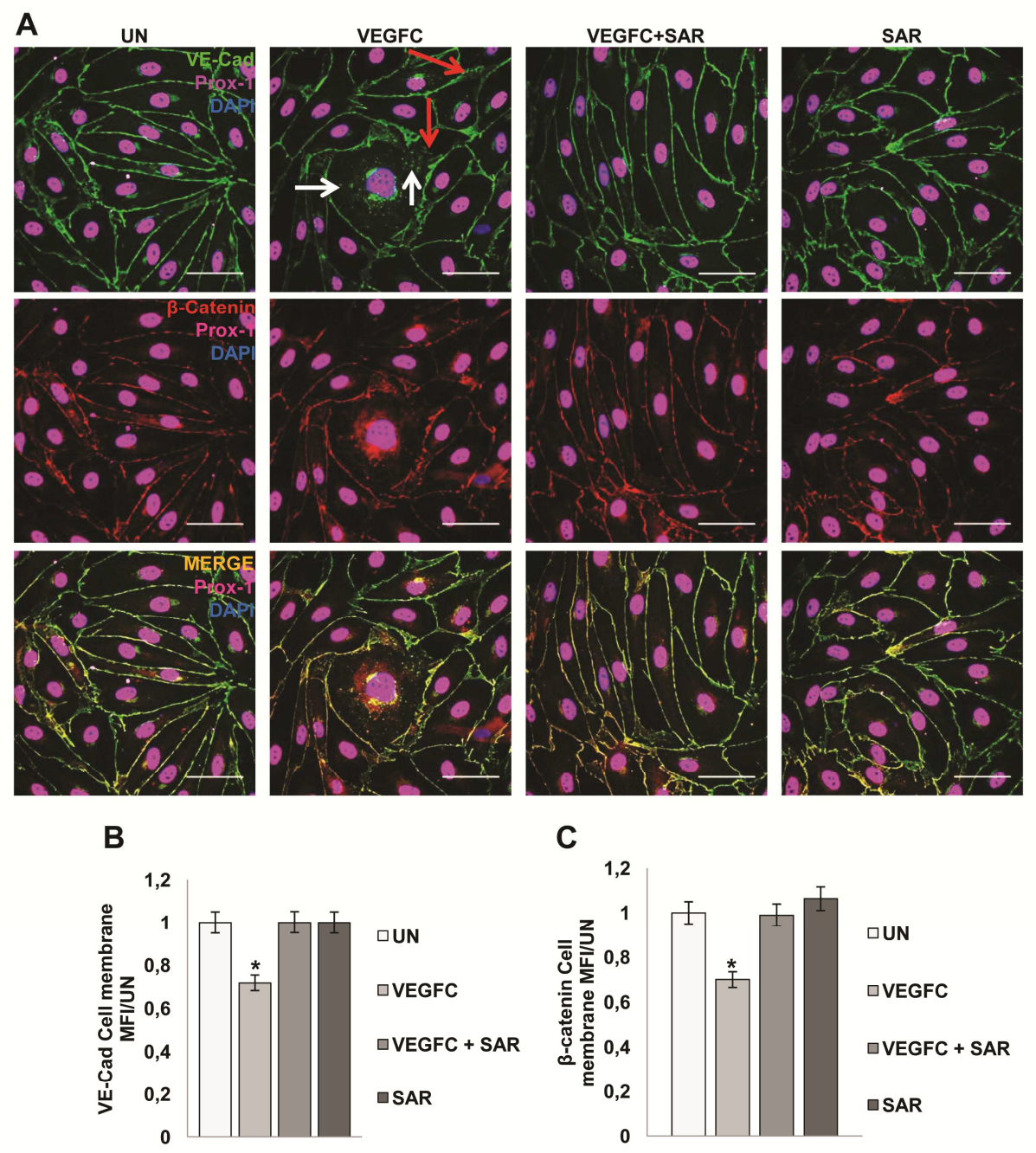
A
UN
VEGFC
VEGFC+SAR
SAR
VE-Cad
Prox-1
DAPI
β-Catenin
Prox-1
DAPI
MERGE
Prox-1
DAPI
B
VE-Cad Cell membrane MFI/UN
1,2
1
0,8
0,6
0,4
0,2
0
*
UN
VEGFC
VEGFC + SAR
SAR
C
β-catenin Cell membrane MFI/UN
1,2
1
0,8
0,6
0,4
0,2
0
*
UN
VEGFC
VEGFC + SAR
SAR

Figure 5

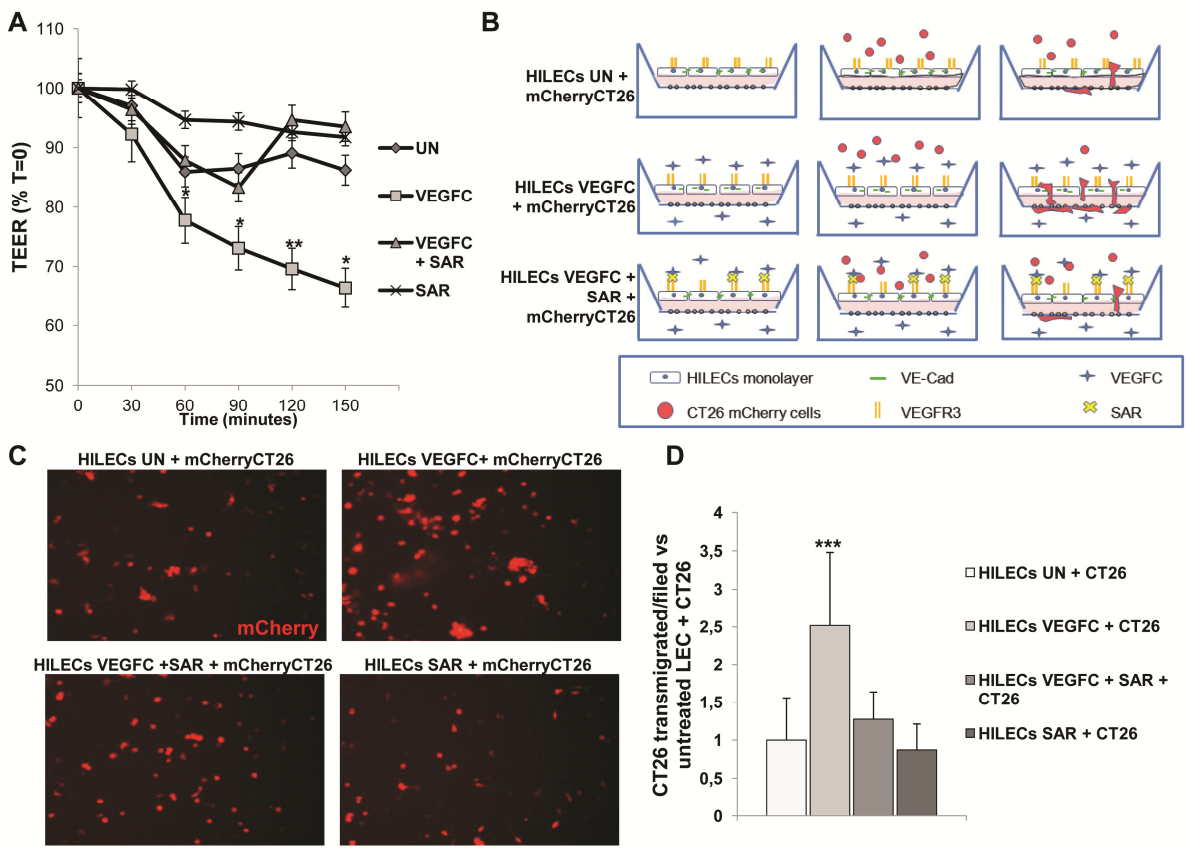

Figure 6

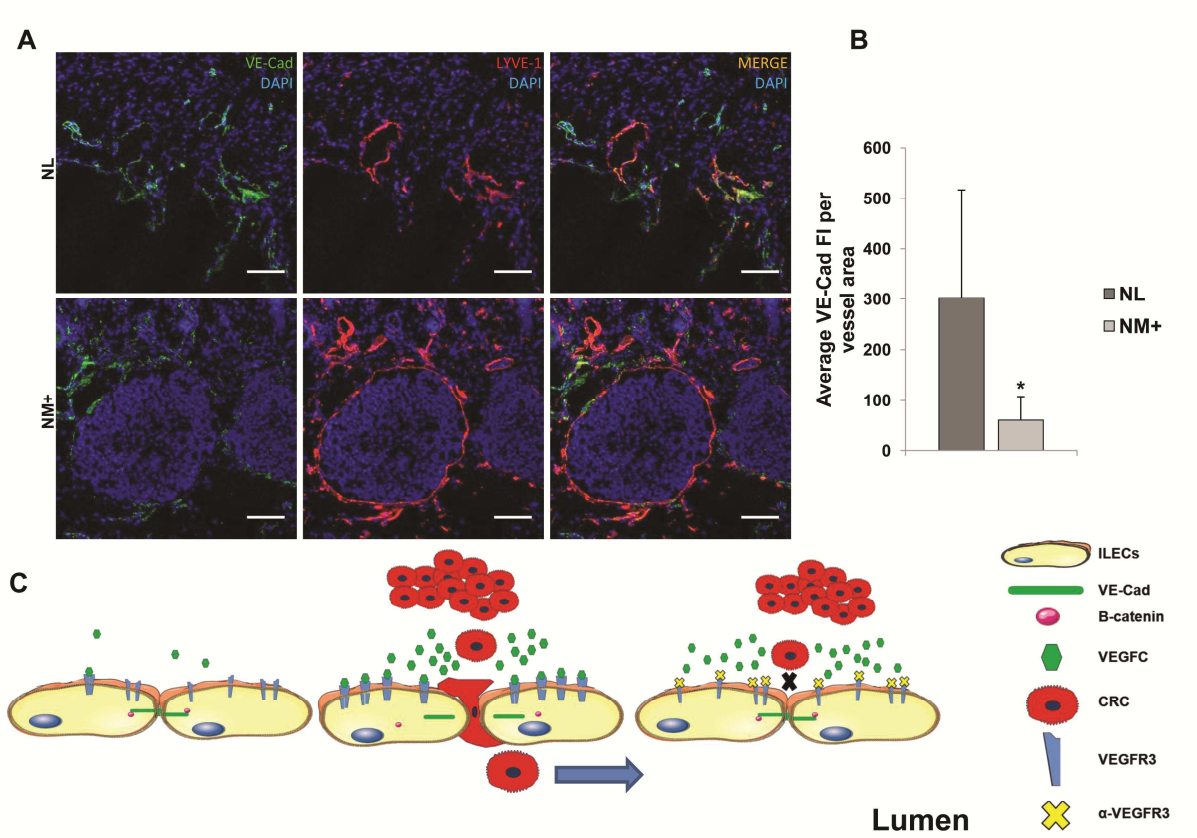

Figure 7

Supplemental Material and Methods

Immunohistochemical staining of Human Colonic Tissues

To quantify lymphatic vessel (LV) density, the number of Podoplanin-positive LVs was assessed in tumor areas of surgical specimens from patients with CRC. Normal areas of the intestine from patients admitted for bowel resection due to diverticulitis or polyps were used as controls (NL, n=15). Tissues were fixed in 4% buffered formalin, processed, and stained with haematoxylin (DAKO) and eosin (Diapath) or immunostained with specific antibodies. Two μm thick sections, of formalin-fixed paraffin embedded tissues were deparaffinised in Bioclear (Bioptica) and rehydrated in a descending ethanol series. Following antigen retrieval by heating 10 minutes in a microwave with EDTA buffer (pH 8.0; 0.25 mM), sections were incubated for 20 minutes with Peroxidased-1 solution (Biocare Medical) to quench endogenous tissue peroxidase. Tissue slides were then incubated for 60 minutes at room temperature in a humid chamber with mouse antihuman Podoplanin monoclonal antibody (clone D2-40; 1:100; ABD Serotec) and staining was completed using the Biocare Medical HRP-conjugated mouse detection kit and diaminobenzidine chromogen as substrate, according to the manufacturer's instructions. Lastly, sections were counterstained with CAT haematoxylin (Biocare Medical) for 5 minutes. After staining, the slides were dehydrated through graded alcohols and mounted with a cover slip using a Eukitt Quick Hardening Mounting Media (Fluka). Negative controls with an omission of the primary incubation were also included. The slides were analyzed randomly by two of the authors, blinded to clinical data.

LV density was quantified in the lamina propria and submucosal layers, both areas richly vascularized by lymphatic capillaries. Only vessels stained with Podoplanin and visible lumina were considered countable, because small nerve fibers and fibroblasts also expressed Podoplanin[1] and potentially could be confused with collapsed lymphatic capillaries. The mean vessel density of 10 areas with an elevated

number of LVs in the 20x magnification objective field, were assessed separately using the VS-ASW software (Olympus).

Real-Time PCR

RNA was extracted from human tumor and healthy specimen or from healthy mouse colon and CT26 cell line using the PureZOL RNA isolation reagent (BIORAD) according to manufactured instructions. RNA retrotranscription was performed with High Capacity cDNA Reverse Transcription Kits (Applied Biosystems®). Real-Time PCR analyzes were performed starting with cDNA obtained from human NM+ tumor (n=13) or healthy (n=13) tissues or from CT26 cell line and mouse colon used as control. The primer pairs used are summarized in the table below:

GENE Product	*Forward PRIMER*	*Reverse PRIMER*
hVEGFC	5'-CTGCCGATGCATGTCTAAAC-3'	5'-CTTGTTCGCTGCCTGACAC-3'
hVEGFD	5'-CAGTACCTGAATTAGTGCCTG-3'	5'-ATAGCATGTCAATAGGACAGAG-3'
hGAPDH	5'-CATGAGAAGTATGACAACAGC -3'	5'-AGTCCTTCCACGATACCAAAG-3'
mVEGFR3	5'-TATGTCCGAAAGGGCAGTG-3'	5'-ACACCTTATCAAAGATGCTCTCG-3'
mVEGFR2	5'-GACCAAGAGTGACCAAGGGG-3'	5'-GATTCGGACTTGACTGCCCA-3'
mVEGFC	5'-GCGCTGATCCCCAGTCCG-3'	5'- AGGACAGACATCAGCTCATC-3'
mGAPDH	5'-CGTGTTCCTACCCCCAATGT-3'	5'-TGTCATCATACTTGGCAGGTTTCT-3'

The reactions were performed on ViiA™7 Real-Time PCR System (Applied Biosystems). GAPDH expression was used as housekeeping gene. Data were calculated using the $2^{\wedge-\Delta Ct}$ method.

Cell line culture condition and infection

The murine colon cancer CT26 cells were kindly provided by Dr. Giuseppe Celesti (Humanitas Clinical and Research Center, Milan, Italy). As demonstrated, the murine colon cancer CT26 cells are highly metastatic to liver and lungs[2]. Cells were maintained in Dulbecco modified Eagle medium (DMEM) supplemented with 10% fetal bovine serum, glutamine, sodium pyruvate, non-essential aminoacids and a penicillin-streptomycin amphotericin mixture (Lonza). Adherent monolayer cultures were maintained on plastic at 37°C in 5% CO_2 and 95% air. All cultures were *Mycoplasma* free.

The lentiviral vector pRRLsin.PPT.hPGK.mcherry_pre (kindly provided by Dr. Marco Erreni, Humanitas Clinical and Research Center, Milan, Italy) was produced by transient transfection of 293T cells according to standard protocols[3]. Briefly, subconfluent 293T cells were co-transfected with 11,7 µg of the transfer plasmid, 3,5 µg of the packaging plasmid, 3,5 µg of envelope plasmid and 5 µg of rev-expressing plasmid (ViraPower™ lentiviral packaging mix, Invitrogen) by Lipofectamine (Invitrogen). After 16 hours medium was changed, and 24 hours later recombinant lentiviral vectors were collected, filtered through 0,22 µm-pore-size cellulose acetate filters and immediately used. After having determined the maximum viral efficiency 10^5 CT26 cells in six-well plates were used. After 24 hours CT26 cells were incubated with complete medium and 48 hours later analyzed for infection efficiency, by LSRFortessa™ cell analyzer (BD Biosciences). CT26 mCherry cells maintained mCherry production for several passages.

VEGFR3 antibody blockade

Mice were given intra-peritoneal injections of an anti-mVEGFR3 antibody, mF431C1, (clone 31C1, ImClone Systems, 800 µg/100 µl of PBS per mouse)[4, 5]. Mice were administered intra-peritoneal injections three times per week for the entire experiment, starting from the first day after CT26 mCherry cell injections. A group of mice were sacrificed at 0, 5, 12, and 19 days after CT26 injection and mucosal extracts were analyzed by western blot for assessment of VEGFR3 inhibition. All experiments were performed in triplicate, using 4-8 mice per experimental group.

Adenoviral human VEGFC administration

Mice were given intra-venous injections of an engineered adenovirus encoding human VEGFC (AdVEGFC), or control virus encoding GFP (AdGFP) (not shown) ($5x10^8$ PFU/mouse; ViraQuest)[5] 7 days before CT26 mCherry cell injections. A group of mice were sacrificed at -7, 5, 12, and 19 days from CT26 injection, and mucosal extracts were analyzed by western blot for assessment of human VEGFC production. Adenoviral preparation was free from contamination with helper viruses, bacteria or lipopolysaccharide. All experiments were performed in triplicate, using 4-8 mice per experimental group.

Tumor dimension

Before being sacrificed mice were anesthetized with 100mg/kg ketamine and 50mg/kg xylazine and fluorescent imaging were performed using a Caliper Xenogen IVIS® Spectrum (Caliper Life Sciences, Hopkinton, MA). A light image was obtained for anatomical orientation and fluorescent imaging was performed to observe mCherry using standard parameters including 12.9 cm field of view to observe three mice simultaneously, excitation filter = 570 nm, emission filter = 620 nm, f-stop 1, pixel binning 8 and 0.5 seconds exposure time. Images were analyzed using Living Imaging software and the Region of Interest (ROI) function. At the indicated time point mice were sacrificed and tumor volume was measured by caliper and calculated with the formula $V = 0.5 \times length \times width^2$.

CT26 proliferation and invasion assay

A crystal violet assay was used to assess CT26 proliferation, as described previously[6]. Briefly, CT26 cells were seeded in 96-well cell culture plates (1×10^3 cells/well) with complete growth medium containing 1% fetal calf serum, and either left untreated or treated with human recombinant VEGFC (100 ng/ml; R&D system) or mF431C1 (300 µg/ml, Imclone). Medium was changed every other day and after 3 days in culture, cells were stained with 0.2% crystal violet (Sigma) dissolved in ethanol.

Uptake of dye by cells on plates was eluted with 33% acetic acid in water. Plates were gently shaken for 20 minutes and the absorbance at 560 nm was measured by a Versamax microplate reader (Molecular Devices) at a wavelength of 560 nm. The optical density of each sample was then compared with a standard curve, in which the optical density was directly proportional to known cell numbers. Invasion assay was assessed by using a BD BioCoat Matrigel invasion chamber with polycarbonate filters (8-μm pore size; BD Biosciences), 24 hours serum starved CT26 $80x10^3$/filter were plated in the upper chamber in DMEM medium, both the upper and the lower chamber were supplemented with human VEGFC (100 ng/ml; R&D system) and/or SAR131675 (23 nM dissolved in DMSO; Selleckchem). After 16 hours, medium was removed from both chambers, and cells that had migrated onto the lower surface of the porous membrane were washed twice in PBS and stained with Diff Quick (Medion Diagnostics), according to the manufacturer's instruction. Triplicates of migrated cells were counted in 5 consecutive fields using a 10x objective. All experiments were performed in triplicate.

Metastasis dissemination assessment

At the indicated time point mice were sacrificed and liver, lungs, and draining lymphnodes were taken for metastasis evaluation by FACS analysis, as previously described[7], and a piece of mCherry tumor was used as a positive control. Briefly organs were disrupted through a 70 μm filter (BD Falcon) with a 1 ml syringe plunger and washed with 10 ml of RPMI medium supplemented with 10% fetal calf serum and 20 mM Hepes. Liver and lungs were then centrifuged at 800 rpm for 10 minutes to discard debris. ACK lysis buffer was used directly on pellets to remove red blood cells. All samples were washed with RPMI medium and centrifuged. Samples were then suspended in PBS and counted. $5x10^6$ cells were stained with LIVE/DEAD® Dead Cell Stain Kit (Life Technologies) and washed in PBS. Stained cells were analyzed using an LSRFortessa™ cell analyzer (BD Biosciences), and data were analyzed using the FACSDiva software (BD Biosciences) considering mCherry positive cells on total living cells. All experiments were performed in triplicate, using 4 mice per experimental group.

Immunofluorescence of human and murine colon tissues

Frozen sections (6 μm) of human (tumor tissue=8; healthy control=8) and murine colon tissues (n=8 per experimental group) were fixed in 4% paraformaldehyde solution for 10 minutes and then permeabilised in 0.1% Triton X-100 solution for 20 minutes at room temperature. Tissue sections were then blocked with PBS containing 2% bovine serum albumin, 0.05% Tween and 2% goat (for human colon tissues) or donkey serum (for murine colon tissue) for 30 minutes at room temperature. After blocking, human colon sections were incubated with mouse anti-VEGFR3 (1:100; Millipore) or mouse anti-VE-Cad (1:50; abcam), and rabbit anti-LYVE-1 (1:200; abcam) antibodies for 2 hours. Murine colon sections were incubated overnight at 4°C with rabbit anti-CD31 (1:100; Life Science Biotechnology) and/or anti-VE-Cad (1:100; eBioscience) and goat anti-LYVE-1 (1:50; R&D systems) primary antibodies. All sections were subsequently incubated for 30 minutes with anti-mouse Alexa Fluor 647-conjugated, anti-rabbit Alexa Fluor 488-conjugated, anti-goat Alexa Fluor 488-conjugated, anti-rat Alexa Fluor 488-conjugated, and anti-rabbit Alexa Fluor 594-conjugated antibodies (1:1000; Molecular Probes), followed by incubation with DAPI for nuclear staining (1:25000; Invitrogen). Sections were mounted with ProLong Gold mounting medium (Invitrogen) and analyzed with a laser scanning confocal microscope (FluoView FV1000; Olympus).

Whole mount staining

Colons were removed from untreated (UN) and treated mice subjected to orthotopic CRC protocol with the indicated treatments (n=5-8 mice each experimental group), and immersed in 1% paraformaldehyde fixative solution, overnight at 4°C. Tissues were then washed and incubated with anti-CD31 (1:500; Millipore), rabbit anti-LYVE-1 (1:500; abcam) and rat anti-VE-Cad (1:200; eBioscience) antibodies diluted in PBS containing 0.3% Triton X-100, 2% bovine serum albumin, 5% goat serum, 0.01% glycine, and 0.1% sodium azide, overnight at 4°C. Anti-hamster Alexa Fluor 647, anti-rabbit Alexa Fluor 594 (1:500; Molecular Probes) and anti-rat Alexa Fluor 488 (1:500; Molecular Probes) were used

as secondary antibodies, and incubated overnight at 4°C. Samples were then mounted with Vectashield (Vector Laboratories) and imaged with a laser scanning confocal microscope (Fluoview FV1000; Olympus).

Morphometric and immunofluorescence intensity measurements

Morphometric analysis of colon whole mounts was performed by 3D visualization of LVs. Images were taken as a z series stack using a 10x objective, and analyzed by Imaris Bitplane software, thus allowing visualization of the LVs in the submucosal and serosal-muscular layers. For each colon analyzed (n=5-8 mice each experimental group), LV density and size were measured in 10 randomly chosen regions covered by vessels (each 1.0 mm^2 in area) and were represented as average number of vessels per area (mm^2) and mean value of diameters (μm), respectively.

The number of LYVE-1-, VEGFR3-, or VE-Cad-positive vessels in single and double-stained murine colon tissues was established by stereological point counting of 10 regions per section (mucosal, submucosal and serosal layers), each 1.5 mm^2 in area, using the FluoView software (Olympus). We considered as LVs only LYVE-1 positive vessel with a visible lumen. Values are expressed as mean number of positive vessels per square millimeter. Analysis of human and mouse VEGFR3 and/or VE-Cad and LYVE-1 double-staining, was performed as described by Tammela et al.[8], with slight modifications. In brief, murine colon sections (n=8 mice each experimental group) were double-stained with rabbit anti-LYVE-1 (1:400; abcam) and rat anti-VE-Cad (1:100; eBioscience) primary antibodies, while staining of human colon sections are described above. Fluorescent images were acquired at a constant exposure time at 20x or 60x magnification on a laser scanning confocal microscope (FluoView FV1000; Olympus). Colons stained with secondary antibodies alone were used to set the exposure time. Vascular structures with a lumen were analyzed with FluoView software (Olympus) and all images were within a linear intensity range between 0 and 6231. To exclude nonspecific staining, structures less than 8 μm (1 μm = 6.8 pixels) in diameter were excluded. To calculate mean vessel

intensity, the sums of pixel intensities per vessel were divided by total vessel area (μm^2). Mean vessel fluorescence intensity (FI) from 5 to 10 images per specimen were averaged and compared between treated and control groups (mouse) and healthy and tumor (human).

Isolation and culture of HILEC and HIBEC

HILEC were obtained from human intestinal microvascular endothelial cells (HIMEC), which were isolated as previously described[5, 9]. Briefly, HIMEC were obtained from normal areas of the intestine of patients admitted for bowel resection of colon cancer, polyps, or diverticulitis (n=10). HIMEC were isolated by enzymatic digestion of intestinal mucosal strips followed by gentle compression to extrude endothelial cell clumps, which adhere to fibronectin-coated plates and were subsequently cultured in MCDB131 medium (Sigma) supplemented with 20 % fetal calf serum, antibiotics, heparin, and endothelial cell growth factor. After 9 days in culture, as previously reported[5], cells were trypsinised and incubated with the following antibodies: anti-human Podoplanin (1 mg per 10^6 cells; Santa Cruz), anti-human VEGFR3 (625 ng per 10^5 cells; R&D system), and PE-conjugated mouse anti-human CD31 antibody (10 µl per 10^6 cells) followed by incubation with Alexa Fluor 647- and Alexa Fluor 488-conjugated secondary antibodies (Molecular Probes). HILEC were then sorted on a FACSAria IIU (BD Biosciences), using a FACSDiva software (version 6.1.3; BD Biosciences), by positive selection for Podoplanin and VEGFR3 gated on a CD31-positive cell population cells (BD Pharmingen) and HIBEC by gating on CD31-positive and Podoplanin and VEGFR3 negative cell population. Cultures of HILEC and HIBEC were maintained at 37°C in 5% CO_2, fed twice a week, and split at confluence. HILEC and HIBEC were used between passages 2 and 6.

HIBEC adenoviral infection

HIBEC were seeded on 6 well plates and infected with AdVEGFC or AdGFP (MOI=500), used as a control, or left untreated in MCDB131 complete medium supplemented with 2% fetal calf serum. After

6 hours medium wash replaced with fresh MCDB131 complete medium supplemented with 20% fetal calf serum and used after 2 days.

Immunoprecipitation and Western Blotting

Human colonic samples from CRC-involved area (n=13) and healthy controls (n=13) or mouse colon tissues from animals with the indicated treatments and at the indicated time points (n=3/group/time) were mechanically homogenized in lysis buffer for protein extraction. Infected HIBECs and controls were scraped in lysis buffer for protein extraction while medium was collected for VEGFC evaluation. Insoluble material was removed by centrifugation for 30 minutes at 14,000 *rpm* at 4°C and the concentration of proteins in each lysate was measured using the Bio-Rad protein assay (Bio-Rad Laboratories). For immunoprecipitation, mouse extracts were pre-cleared with lysis buffer-containing protein-G agarose beads for 1 hour at 4°C. Pre-cleared lysates (1 mg) were incubated with an antibody against mouse VEGFR3 (1 μg/ml in lysis buffer; R&D system) overnight at 4°C. After washing with lysis buffer, the immunoprecipitates were resuspended in 50 μl of SDS-sample buffer, incubated at 95°C for 5 minutes and immunoblotted, as described below.

Proteins (80 μg for tissue homogenate and 50 μg for cell lysates), cell culture medium (50 μl) and immunoprecipitates were separated on a 10% Tris-glycine gel and electrotransferred to a nitrocellulose membrane (Bio-Rad Laboratories). Nonspecific binding was blocked with Tris-buffered saline (TBS) containing 5% non-fat dried milk and 0.1% Tween 20, followed by overnight incubation at 4°C with the rabbit anti-human VEGFR3 antibody (1:500; Life Technologies), the rabbit anti-human VEGFC antibody (1:1000; abcam), and an anti–actin antibody (1:1000; Santa Cruz Biotechnology) as loading control. Mouse anti-phosphotyrosine (1:1000; Millipore) and anti-mouse VEGFR3 (1:500; ImClone Systems) antibodies were used to visualize immunoprecipitated samples. Membranes were washed for

1 hour with TBS containing 0.1% Tween 20 and then incubated for 1 hour with the appropriate horseradish peroxidase-conjugated secondary antibody (1:3000; GE Healthcare). The membranes were then incubated with Immobilon Western Chemilum (Millipore) for 1 minute, after which bands were detected by Chemidoc (Bio-Rad Laboratories), using Quantity One software.

Tubule formation assay, migration assay and proliferation assay

HIBEC tube formation was assessed using Matrigel (BD Biosciences) as previously describe[5]. Briefly, multiwell dishes were coated with 250 μL of complete medium containing 5 mg/ml Matrigel for 30 minutes at 37°C HIBEC were seeded in triplicate at a density of 5×10^4 in complete MCDB131 medium infected with AdVEGFC, AdGFP or untreated. Cells were cultured on Matrigel for 4 hours, and inverted phase-contrast microscopy was used to assess and count endothelial tube-like structures. Five high-power fields per condition were examined. All experiments were repeated three times.

Migration assay was assessed as previously reported[9], with some modifications. By using a BD BioCoat Matrigel invasion chamber with polycarbonate filters (8μm pore size; BD Biosciences), starved (MCDB131 for 18 hours) HIBEC (50 x 10^3/filter) were plated in the upper chamber in MCDB131 medium. After 18 hours, medium was removed from both chambers, and cells that had migrated onto the lower surface of the porous membrane were washed twice in PBS and stained with Diff Quick (Medion Diagnostics), according to the manufacturer's instruction. Triplicates of migrated cells were counted in the entire membrane using a 20x objective. Proliferation for HIBEC was evaluated as described above for CT26 cells with brief modifications. Briefly, HIBEC were seeded in 96-well cell culture plates (1×10^3 cells/well) with MCDB131 medium. HIBEC were previously infected with AdVEGFC, AdGFP or not infected. Medium was changed every other day and after 4 days in culture, cells were stained with 0.2% crystal violet (Sigma) dissolved in ethanol. Uptake of dye

by cells on plates was eluted with 33% acetic acid in water. Plates were gently shaken for 20 minutes and the absorbance at 560 nm was measured by a Versamax microplate reader (Molecular Devices) at a wavelength of 560 nm. The optical density of each sample was then compared with a standard curve, in which the optical density was directly proportional to known cell numbers.

HILECs immunofluorescence and evaluation of VE-Cad internalization

Serum starved (MCDB131 for 24 hours) confluent HILEC were left unstimulated or stimulated with VEGFC (100 ng/ml; R&D system) and/or SAR131675 (23 nM dissolved in DMSO; Selleckchem) for 30 minutes in starving medium. HIBEC infected for AdVEGFC, AdGFP or not infected were serum starved for 1 hour. Cells were fixed with 4% paraformaldehyde fixative solution for 10 minutes at room temperature, washed with PBS and blocked and permeabilized with 5% fetal calf serum, 5% human serum, 2% bovine serum albumin, 0.1% Triton X-100 solution for 30 minutes at room temperature. After blocking, HIBEC were incubated with mouse anti-VE-Cad (1:100; BD Bioscience), rabbit anti-β-catenin (1:600; abcam), and HILECs also with goat anti-Prox1 (1:80; R&D systems) antibodies overnight at 4°C. After washing HILECs were subsequently incubated for 1 hour with anti-goat Alexa Fluor 647-conjugated, anti-rabbit Alexa Fluor 594-conjugated and anti-mouse Alexa Fluor 488-conjugated antibodies (1:1000; Molecular Probes), and HIBEC with anti-rabbit Alexa Fluor 594-conjugated and anti-mouse Alexa Fluor 647-conjugated antibodies followed by incubation with DAPI for nuclear staining (1:25000; Invitrogen) for 10 minutes at room temperature. Cover glasses were mounted with ProLong Gold mounting medium (Invitrogen) and. Fluorescent images were acquired at a constant exposure time at 60x magnification on a laser scanning confocal microscope (FluoView FV1000; Olympus). To calculate mean membrane intensity, the sums of pixel intensities per cell membrane were subtracted from inner membrane pixel intensities. Mean membrane fluorescence intensity (FI) from 10 images per treatment were averaged and compared between treated and control

groups. VE-Cad internalization experiments were performed in triplicates and are the result of 3 independent experiments.

HILEC permeability assay

HILECs were seeded on fibronectin coated 0.4 μm pore-size Transwell Permeable Supports (Corning Costar, Cambridge, MA), cultured in complete culture medium and let to form a monolayer, as previously described[10]. After the establishment of a stable monolayer HILECs were serum starved for 24 hours and then were stimulated with VEGFC (100 ng/ml; R&D system) and/or with SAR131675 (23 nM dissolved in DMSO; Selleckchem) and assayed for permeability using a Millicall-ERS voltohmmeter (World Precision Instruments, New Haven, CT) to measure the transendothelial electrical resistance (TEER) as previously described. The percentage of change in the TEER was calculated with respect to time 0 for each indicated time point. Experiments were performed in triplicates and are the result of 3 independent experiments.

Transendothelial migration assay

BioCoat Matrigel invasion chamber with polycarbonate filters (8-μm pore size; BD Biosciences) were seeded with HILECs or HIBECs in complete medium. After the establishment of a stable monolayer HILECs were stimulated with VEGFC (100 ng/ml; R&D system) and/or with SAR131675 (23 nM dissolved in DMSO; Selleckchem) for 24 hours. HIBECs infected with AdVEGFC or GFP or untreated were cultured in complete medium to establish a stable monolayer. MCherry CT26 cells were trypsinised, counted and plated on top of HILEC monolayer in the presence of VEGFC (100 ng/ml; R&D system) and/or SAR131675 (23 nM dissolved in DMSO; Selleckchem) or on HIBECs in complete medium. After 16 hours mCherry CT26 transmigrated cells were counted in 5 consecutive fields with a 10x zoom fluorescent microscope. Experiments were performed in triplicates and are the result of 3 independent experiments.

Supplemental Figure Legend:

Supplementary Figure 1

Mice receiving mCherry CT26 ortothopic injection were administered with an adenovirus encoding hVEGFC (n=3/time point), or anti-VEGFR3 antibody (mF431C1, n=3/time point). (**A**) Colonic samples from healthy and tumor-bearing mice with the indicated treatments and at the indicated time points were mechanically homogenized in lysis buffer for protein extraction. Representative blots for immunoprecipitation and immunoblotting are shown. Days are relative to CT26 injections. (**B-E**) HIBEC were infected with AdVEGFC, AdGFP or not infected. (**B**) Western blot performed on cell lysates or medium demonstrated that VEGFC was produced at low levels by HIBEC and it was efficiently secreted when cells were infected with AdVEGFC. HIBEC infected with AdVEGFC, AdGFP or left untreated (UN) displayed comparable proliferation (**C**), migration (**D**) and capillary formation (**E**). Results are representative of three independent experiments each in triplicate/group. Values are expressed as Mean ±SD. (**F**) Representative images of colonic whole mount staining of mice without tumor (WT) and groups administered with adenoviruses encoding hVEGFC, or anti-VEGFR3 antibody (mF431C1) stained for LYVE-1 (green) and VE-Cad (red). WT group (left upper panel), is visible the canonical "button and zippers" VE-Cad distribution; AdVEGFC-injected group, revealed a discontinuous VE-Cad LVs' distribution; VEGFR3 inhibition with mF431C1 increased VE-Cad on LVs. Lower panels are higher magnifications of the white dashed squares in the upper panel. Scale bar: 50µm.

Supplementary Figure 2

(**A**) Representative merges of HIBECs stained for DAPI (blue), β-catenin (red) and VE-Cad (white) or expressing GFP (green). Cells were not infected (UN) or infected with AdVEGFC or AdGFP displayed similar VE-Cad and β-catenin distribution. Scale bar: 50µm. Transendothelial migration assay:

mCherry-CT26 cells were seeded on HIBEC confluent monolayers not infected, infected with AdVEGFC or with AdGFP. MCherry-positive transmigrated cells were counted (**B**). Results are representative of three independent experiments each in triplicate/group and values are expressed as Mean ±SD.

References:

1. Schacht V, Dadras SS, Johnson LA, et al. Up-regulation of the lymphatic marker podoplanin, a mucin-type transmembrane glycoprotein, in human squamous cell carcinomas and germ cell tumors. Am J Pathol 2005;166:913-21.
2. Schackert HK, Fidler IJ. Development of an animal model to study the biology of recurrent colorectal cancer originating from mesenteric lymph system metastases. Int J Cancer 1989;44:177-81.
3. Dull T, Zufferey R, Kelly M, et al. A third-generation lentivirus vector with a conditional packaging system. J Virol 1998;72:8463-71.
4. Pytowski B, Goldman J, Persaud K, et al. Complete and specific inhibition of adult lymphatic regeneration by a novel VEGFR-3 neutralizing antibody. J Natl Cancer Inst 2005;97:14-21.
5. D'Alessio S, Correale C, Tacconi C, et al. VEGF-C-dependent stimulation of lymphatic function ameliorates experimental inflammatory bowel disease. J Clin Invest 2014.
6. Vega-Avila E, Pugsley MK. An overview of colorimetric assay methods used to assess survival or proliferation of mammalian cells. Proc West Pharmacol Soc 2011;54:10-4.
7. Enquist IB, Good Z, Jubb AM, et al. Lymph node-independent liver metastasis in a model of metastatic colorectal cancer. Nat Commun 2014;5:3530.
8. Tammela T, Petrova TV, Alitalo K. Molecular lymphangiogenesis: new players. Trends Cell Biol 2005;15:434-41.
9. Scaldaferri F, Vetrano S, Sans M, et al. VEGF-A links angiogenesis and inflammation in inflammatory bowel disease pathogenesis. Gastroenterology 2009;136:585-95 e5.
10. Breslin JW, Yuan SY, Wu MH. VEGF-C alters barrier function of cultured lymphatic endothelial cells through a VEGFR-3-dependent mechanism. Lymphat Res Biol 2007;5:105-13.

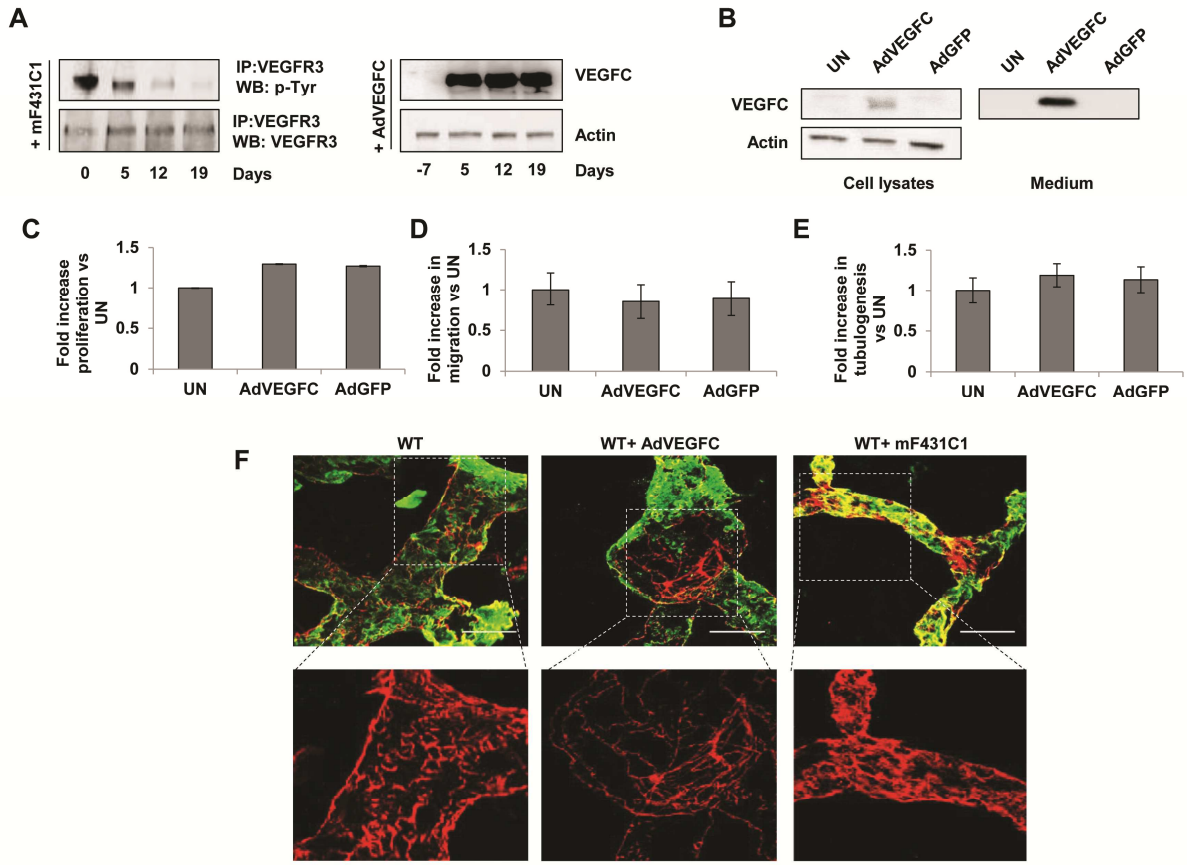

Supplementary Fig. 1

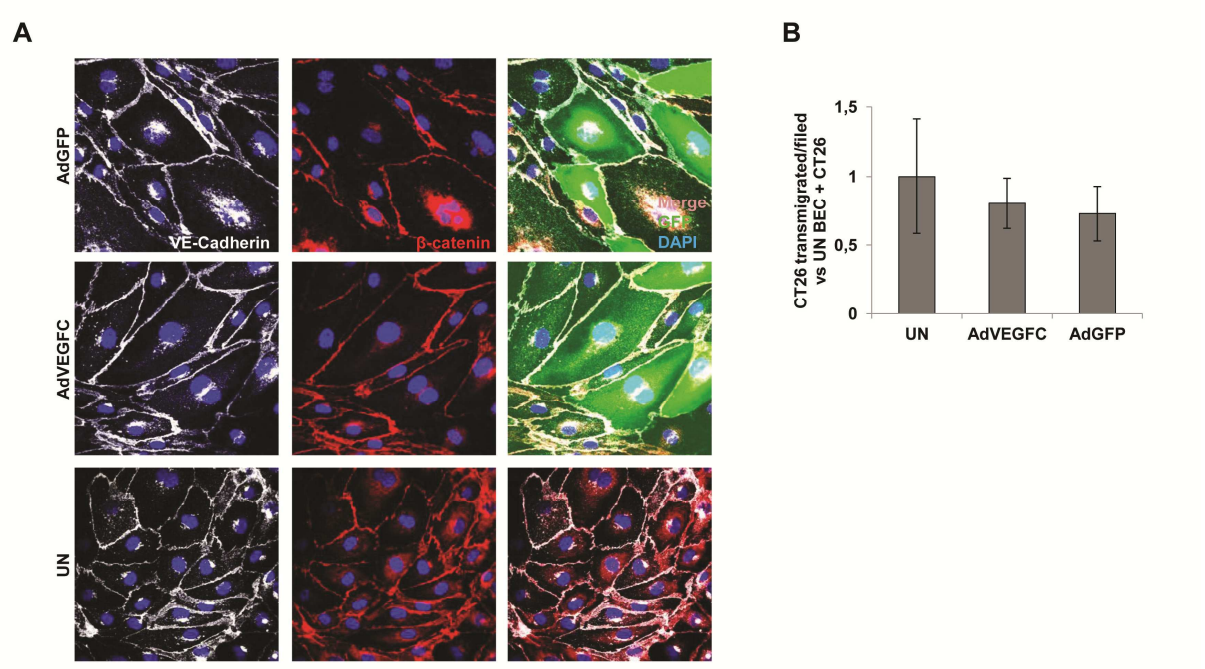

Supplementary Fig. 2